



Quantitative cervical spine injury responses in whiplash loading with a numerical method of natural neural reflex consideration

Ziyang Liang^{a,b}, Fuhao MO^{a,*}, Zhefen Zheng^a, Yuandong Li^a, Ye Tian^a, Xiaobing Jiang^c, Tang Liu^b

^a College of Mechanical and Vehicle Engineering, Hunan University, Changsha, Hunan 410082, China

^b Department of Orthopedics, The Second Xiangya Hospital of Central South University, Changsha, Hunan 410011, China

^c Department of Spine Surgery, Guangzhou University of Chinese medicine, Guangzhou, Guangdong 510405, China

ARTICLE INFO

Article history:

Received 12 August 2021

Revised 7 March 2022

Accepted 15 March 2022

Keywords:

Cervical spine injuries

Neural reflex

Finite element method

Neuromuscular

Whiplash

ABSTRACT

Background and objective: Neural reflex is hypothesized as a regulating step in spine stabilizing system. However, neural reflex control is still in its infancy to consider in the previous finite element analysis of head-neck system for various applications. The purpose of this study is to investigate the influences of neural reflex control on neck biomechanical responses, then provide a new way to achieve an accurate biomechanical analysis for head-neck system with a finite element model.

Methods: A new FE head-neck model with detailed active muscles and spinal cord modeling was established and globally validated at multi-levels. Then, it was coupled with our previously developed neuromuscular head-neck model to analyze the effects of vestibular and proprioceptive reflexes on biomechanical responses of head-neck system in a typical spinal injury loading condition (whiplash). The obtained effects were further analyzed by comparing a review of epidemiologic data on cervical spine injury situations.

Result: The results showed that the active model (AM) with neural reflex control obviously presented both rational head-neck kinematics and tissue injury risk referring to the previous experimental and epidemiologic studies, when compared with the passive model (PM) without it. Tissue load concentration locations as well as stress/strain levels were both changed due to the muscle activation forces caused by neural reflex control during the whole loading process. For the bony structures, the AM showed a peak stress level accounting for only about 25% of the PM. For the discs, the stress concentrated location was transferred from C2-C6 in the PM to C4-C6 in the AM. For the spinal cord, the strain concentrated locations were transferred from C1 segment to around C4 segment when the effects of neural reflex control were implemented, while the gray matter and white matter peak strains were reduced to 1/3 and 1/2 of the PM, respectively. All these were well correlated with epidemiological studies on clinical cervical spine injuries.

Conclusion: In summary, the present work demonstrated necessity of considering neural reflex in FE analysis of a head-neck system as well as our model biofidelity. Overall results also verified the previous hypothesis and further quantitatively indicated that the muscle activation caused by neural reflex is providing a protection for the neck in impact loading by decreasing the strain level and changing the possible injury to lower spinal cord level to reduce injury severity.

© 2022 Elsevier B.V. All rights reserved.

1. Introduction

Cervical spine stabilizing system is composed of passive characteristics of the osteoligamentous spine and the active neuromuscular system [1–4]. The basic premise of this landmark theoretical hypothesis is that the neural element is a regulating step in

this stabilizing system [1,4–6]. The neural reflex of peripheral sensory system, represented by vestibular system and muscle-tendon proprioceptors, does attempt to control muscles dynamics during head-neck movements [7–11]. The sensory information from the vestibular system is responsible for providing the brain with motion, head position, and spatial orientation, it is also involved with motor functions that keep balance, stabilize head-neck during movement, and maintain posture [12,13]. In addition, neck muscles are richly endowed with proprioceptors, which are highly sensitive

* Corresponding author.

E-mail address: fuhamoto@hnu.edu.cn (F. MO).

to head yaw rotation [14]. For example, muscle spindles play an important role in regulating the contraction of muscles, by activating motor neurons via the stretch reflex to resist muscle stretch [15,16].

Finite element (FE) human body models (HBMs) are largely established and employed to analyze human body injury mechanisms and treatments. In the last two decades, several human head-neck models have been developed from the cervical spine model without muscles to the model with passive muscles, then the model with stabilizing strategy consideration of active muscles [17–25]. Yang et al. first developed a FE neck model with passive muscles represented by 60 spring elements [17]. Subsequently, Deng et al. established a cervical spine model that contained 15 pairs of active muscles represented by contractile beam elements with Hill muscle material [18]. Then, several detailed FE head-neck models or FE whole-body models including the head-neck component were developed for injury analysis, such as the KTH model [19], the ViVA openHBM [23], the THUMS model [20], and the GHBMC model [21,22].

Recently, few studies involved modeling methods of neural reflex control in HBMs. Putra et al. implemented a PID (Proportion-Integral-Derivative)-based control strategy in the ViVA female OpenHBM that was first established by Östh et al., which included an angle-based and length-based active muscle controller [23,26,27]. This simplified sensory feedback control modeling method was indicated to be limit in reacting to environmental perturbation [28]. In early stage, our research group developed a Human Active Lower Limb (HALL) model with PID control strategy [29,30]. Happee et al. developed a head-neck multibody model with vestibulocollic reflex and cervicocollic reflex, but it did not investigate the response under impact load [31]. In our recent studies, a lower limb musculoskeletal model with proprioceptive reflex loop and ascending signals was developed with proved perturbation resistance ability, and applied in gait analysis [32,33]. In a further step, we developed a neuromuscular head-neck model with vestibular and proprioceptive reflex control loops, and applied it in impact analysis that demonstrated significant influences of these proprioceptors in head-neck dynamic responses [34]. However, the musculoskeletal model cannot easily and accurately obtain tissue stress and strain distribution for detailed injury risk analysis due to its theoretical limitation.

Therefore, the purpose of this study is to quantitatively analyze the effects of neural reflex on neck injury risk, and verify them by comparing a review of epidemiologic studies on cervical spine injuries, in that case to provide a new way to achieve an accurate biomechanical analysis for the head-neck system with a FE model. A new head-neck FEM with active muscles and spinal cord was first developed, and validated from isolated tissues to the segments and the whole cervical spine. Then, we combined it with our previously developed neuromuscular model to analyze the effects of neural reflex on neck injury risk in a typical spinal injury loading condition (whiplash motion), which is a result of sudden acceleration-deceleration movements, and characterized by the lower cervical spine is forced into extension (more lordosis) while the upper cervical spine tends to go into flexion (more kyphosis) [35]. It is probably during this motion sequence that the whiplash injury occurs. As the motion progresses, the whole cervical spine is finally hyperextended. Whiplash injuries manifest in a range of symptoms that have been given the common term whiplash associated disorders (WADs) [36]. The set of symptoms are well documented and classified in The Quebec Task Force Classification of Grades of WADs [37]. Examples include neck pain, intervertebral disk injury, and neurological signs. In addition, this study also verified the obtained effects by comparing a systematic review of epidemiologic data on cervical spine injuries.

2. Methods

2.1. Development of FE head-neck model with active muscles

2.1.1. Geometry reconstruction

The geometry reconstruction of the model was based on a volunteer (169.0 cm height and 67.85 kg weight) with an anthropometry close to the 50th percentile Chinese male as shown in Fig. 1. This study was approved by the First Affiliated Hospital of Guangzhou University of Chinese Medicine committee for clinical research (NO. JY[2020]283), and informed consent was obtained from the volunteer. The sagittal alignment parameters of the cranial vertebra-cervical spine were measured and assessed by clinical authors in X-ray sagittal view (Fig. 1A). The C0-C2 angle, C2-C7 Cobb angle, C2-C7 cervical sagittal angle, and T1 slope were all within the normal range of a healthy adult [38,39]. Then, the geometry of bony structures was extracted from the low-dose computed tomography (CT) scans. Soft tissue structures, such as brain-spinal cord and intervertebral discs, were primarily reconstructed on the basis of the 3.0T magnetic resonance imaging (MRI) scans with an axial interval at 0.7 mm, and 0.88 mm intervals in both sagittal and coronal planes. Medical engineering software Mimics was used to extract the model geometry and followed by geometric processing with the Geomagic software.

2.1.2. Mesh generation and modeling

Mesh generation and modeling was made in Hypermesh software. The generation process in combination with an appropriate mesh resolution allows preservation of morphological features of the biological tissue in the model. The overall FE head-neck model was developed using LS-dyna codes (version 11.1.0 × 64, simple precision, SMP) as shown in Fig. 1. Element type selections were illustrated in Table 1.

Functional spinal unit (FSU). Bony structures were modeled by combining shell and solid elements. The cortical bones of each vertebra were modeled with triangular elements to accurately fit the anatomy features, while their thicknesses were based on the measured cadaver data summarized in the literature [40]. Cancellous bones inside the vertebra were modeled with tetrahedral elements through filling the volume formed by the cortical bones. The zygapophyseal joint cartilages and bony endplates of the model were generated based on vertebrae landmarks and anatomical descriptions [41,42]. The intervertebral discs included the components of annulus fibrosus matrix, nucleus pulposus and annular fibers, which were respectively modeled with hexahedral bulk elements or quadrilateral membrane elements [43]. The intervertebral discs were tied to the adjacent vertebral endplates. The modeling details of fiber layers were referred to the way of Östh et al. and Shen et al. [23,44] studies. The cartilaginous endplates were attached to the disk surfaces in the cranial-caudal direction.

Spinal ligaments. In the lower cervical spine (LCS), from C2 to T1, the anterior longitudinal ligament (ALL), posterior longitudinal ligament (PLL), ligamentum flavum (LF), interspinous ligament (ISL), and facet capsular ligaments (FCL) were modeled with quadrilateral membrane elements based on anatomical descriptions [41,42]. The upper cervical spine (UCS) ligaments from occipital bone to C2 adopted the same modeling method as the LCS ligaments, which included the transverse ligament (TL), tectorial membrane (TM), apical ligament, alar ligaments, atlanto-axial FCL (C1-C2 FCL), and atlanto-occipital FCL (Skull-C1 FCL), anterior (AAAM) and posterior (PAAM) atlanto-axial membrane, anterior (AAOM) and posterior (PAOM) atlanto-occipital membrane, and C1-C2 ALL. They were created based on anatomical insertion sites [41,42,45].

Spinal cord. The spinal cord was modeled by including white and gray matters, denticulate ligaments, pia mater, and dura mater. The white matter (WM) and gray matter (GM) were meshed us-

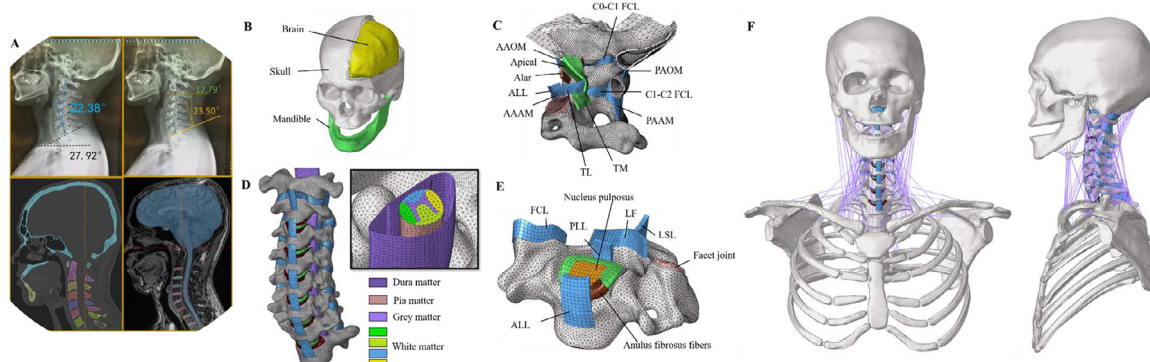


Fig. 1. Views of the FE human active head-neck (HAHN) model. A. X-ray imaging evaluation with subsequent CT/MRI scans. B. Head part with the brain exposed. C. Occipital-atlas-axis unit of the upper cervical spine. D. Whole cervical spine with the spinal cord visible. E. Spinal function unit of the low cervical spine. F. Overall musculoskeletal structure of the whole model.

ing tetrahedral elements. Quadrilateral membrane elements were used for the modeling of pia mater, dura mater, and denticulate ligaments. The pia mater was modeled as an external surface of the WM. The dura mater geometry was referring to Baily et al. study [46]. The nerve roots were not included in the model, and the holes in the dura mater corresponding to root sleeves were filled. The denticulate ligaments were attached along the lateral sides of the pia mater and to the dura mater between each vertebral foramen [46–48].

Muscle. Cervical spine muscles were connected to the bony structures of the head-neck model, which included passive and active properties. 106 pairs of Hill-type 1D elements were used to represent 32 muscle pairs in the cervical spine. The muscle fascicles were redirected at intermediate vertebrae to better follow the curvature of the spine.

2.1.3. Material properties

The material properties of the model were based on the previous literature as shown in Table 1. An isotropic elastic-plastic material was used to model the cortical bones, cancellous bones and bony endplates of the cervical vertebrae [21,22,44,49]. The skull, mandible, hyoid bone, and thoracic vertebrae were modeled as rigid bodies to reduce the computing cost of the present model. The nucleus pulposus was modeled with an elastic fluid material [44]. The annulus was built by a multi-part material consisting of an annulus fibrosus matrix in Mooney-Rivlin material [49], and annular fibers in nonlinear orthotropic characteristics [23]. The UCS and LCS ligaments were represented with different anatomical thicknesses and using orthotropic nonlinear elastic material as indicated by the previously published studies [21–23]. For the spinal cord, the WM and GM were using hyper-elastic Ogden material model based on the recent in-vivo experimental studies on non-human primates [50–52]. The dura matter and pia matter were assigned a linear elastic material with elastic modulus of 5 MPa and 2.3 MPa, respectively [47]. The facet cartilage was also modeled using a linear elastic material with an elastic modulus of 10 MPa [53].

Cervical spine muscles were added to the head-neck model, and defined by the improved Hill model. Detailed data such as origin and insertion points, physiological cross-sectional areas (PCSA), and muscle segment parameters were available in the previous comprehensive dissection studies [54–57]. Muscle passive properties were referred to the previous studies [58,59], while the active contraction force produced by the muscle was determined as follows.

$$F^{CE} = A(t) \cdot F_l(l) \cdot F_v(v) \cdot F_{max} \quad (1)$$

Where $A(t)$ is the muscle activation level, $F_l(l)$ is the normalized force-length curve, $F_v(v)$ is the force-velocity curve, and F_{max} is the maximum isometric force. F_{max} of each muscle was defined by the product of the corresponding PCSA and a normalized stress. The normalized stress value in hyoid muscles was defined as 0.35 MPa based on the Mortensen et al. study [60], and the rest muscles adopted 0.5 MPa [59,61,62]. The calculated F_{max} of each muscle were shown in the Appendix Table 1.

2.2. Model validation

The validation matrix of the head-neck model is illustrated in Table 2. The model was first verified in anatomy measurements. Then, it was validated step by step from isolated tissues or units to the segments and the whole head-neck model. For all conducted simulations, gravity loading (a volume load of 9.81 m/s^2) was included. Simulation details were described as follows.

Anatomy measurements. Vertebral body and overall vertebrae dimensions of the model were compared with human subject data from Vasavada et al. [63]. The verification of model dimensions included vertebral height, vertebral depth, vertebral width, and spinous process length.

Isolated tissues. The spinal cord was validated with the previous indentation tests [51,64]. An impactor was defined as a rigid body and positioned at the level of dorsal left horn of the gray matter at C4 level. A dorsoventral displacement was applied to the impactor at a speed of 0.12 mm/ms. The simulated force-displacement curve was compared with the experimental corridor. Tension tests were performed in all spinal ligaments of the UCS and LCS, where the respective force-displacement simulation curves were compared with the experimental data from Myklebust et al. [65] and Mattucci et al. [66,67].

Functional Spinal Units. First, referring to Shea et al. [68], a uniform axial displacement of 1 mm to the superior nodes of vertebral body was performed to evaluate the FSUs' stiffnesses. Then, motion characteristics of the model were verified in three rotation directions according to the previous studies [69–72]. For FSUs of each segment, moments were applied to the superior portion of the cranial vertebral body in ramped steps of 0.5 Nm for flexion-extension as the previous studies [69–71]. 1 Nm moments were used for lateral bending and axial rotation in accordance with the load increments of the Panjabi et al. study [72].

Whole head-neck model of passive muscles-FE model (PM-FEM). To verify biomechanical responses of the whole head-neck model, we validate the model following White et al. study [73]. An impact acceleration of 4 g was given to a rigid sled with a post mortem human subject (PMHS) in the posterior-anterior direction. Before the simulation, the Frankfort plane was adjusted to align with the

Table 1

Summary of material and element properties used for the head-neck model.

Component	Element type	Constitutive model	Material parameters	Shell thickness (mm)	References
Cortical bone	Triangular shell	Isotropic elastic-plastic	$E = 12.0 \text{ GPa}$ $G = 1.25 \text{ GPa}$ $\sigma_{yield} = 189.8 \text{ MPa}$ $\nu = 0.3$	$C1-C3 = 0.51$ $C4 = 0.55$ $C5 = 0.62$ $C6 = 0.66$ $C7 = 0.70$ $T1-T6 = 0.30$	[21,22,44,49]
Cancellous bone	Tetrahedral	Isotropic elastic-plastic	$E = 442 \text{ MPa}$ $G = 51 \text{ MPa}$ $\nu = 0.3$	N/A	[21,44,49]
Bony endplate	Triangular shell	Isotropic elastic-plastic	$E = 5.6 \text{ GPa}$ $G = 0.3 \text{ GPa}$ $\sigma_{yield} = 36.7 \text{ MPa}$ $\nu = 0.3$	0.5	[21,22]
Nucleus pulposus	Hexahedral	Elastic fluid	$k = 1.72 \text{ GPa}$	N/A	[44]
Annulus fibrosus matrix	Hexahedral	Mooney-Rivin	$A = 0.18$ $B = 0.045$	N/A	[49]
Annulus fibrosus fibers	Quadrilateral membrane	Orthotropic nonlinear elastic	$E_c = 0.01-7.1 \text{ MPa}$ $v_{ab} = 0.3$ $v_{ca} = v_{cb} = 0.49$	0.25	[23]
LCS ligaments	Quadrilateral membrane	Orthotropic nonlinear elastic	$E_c = 0.4-23.3 \text{ MPa}$ $v_{ab} = 0.3$ $v_{ca} = v_{cb} = 0.49$	ALL = 1.5 PLL = 1.7 LF = 1.3 FCL = 1.1 ISL C2-C5 = 1.4 ISL C6-T1 = 1.0	[21,22,23]
UCS ligaments	Quadrilateral membrane	Orthotropic nonlinear elastic	$E_c = 0.65-43 \text{ MPa}$ $v_{ab} = 0.3$ $v_{ca} = v_{cb} = 0.49$	TL = 2.0 TM = 2.5 Alar = 2.9 Apical = 3.0 PAOM = 0.9 AAOM = 0.9 PAAM = 0.9 AAOM = 0.9 CO-C2 FCL = 1.1	[21,22,23]
white matter	tetrahedral	ogden with prony series	$\mu = 0.033 \text{ mpa}$ $\alpha = 3.99$ $k = 0.636 \text{ mpa}$ $G_1 = 0.209 \text{ mpa}$ $G_2 = 0.113 \text{ mpa}$ $G_3 = 0.061 \text{ mpa}$ $G_4 = 0.033 \text{ mpa}$ $t_1 = 1e+02 \text{ ms}$ $t_2 = 1e+03 \text{ ms}$ $t_3 = 1e+04 \text{ ms}$ $t_4 = 1e+05 \text{ ms}$	n/a	[50,51]
gray matter	tetrahedral	ogden with prony series	$\mu = 1.46e-03 \text{ mpa}$ $\alpha = 7.52$ $k = 0.0531 \text{ mpa}$ $G_1 = 1.069 \text{ mpa}$ $G_2 = 0.416 \text{ mpa}$ $G_3 = 0.335 \text{ mpa}$ $t_1 = 6.4e+02 \text{ ms}$ $t_2 = 6.4e+03 \text{ ms}$ $t_3 = 6.4e+04 \text{ ms}$	n/a	[50,51]

N/A: Not applicable; E : Elastic modulus; G : Shear modulus; σ_{yield} : Yield stress; ν : Poisson's ratio; k : Bulk modulus; E_c : Curve of elastic modulus; A , B , μ , α : Material constants.

Table 2

Summary of validation matrix for the FE head-neck model.

Items	Loading types	Loading directions	Experimental references	Validation indexes
Anatomic measurements	Measurement	N/A	[63]	Vertebral height, depth, and width; Spinous process length
Isolated tissues	Spinal cord Spinal ligaments	Compression test Tension test	Vertical axis Vertical axis	Force - Displacement Force - Displacement
Segments	FSUs Range of motion	Compression test 6 DOF moment	Vertical axis Flx/Ext/LB/AR	Force - Displacement Angle - Moment
Whole head-neck	Range of motion	Dynamic rear impact	P-A	Head angle - Time

*Notes: N/A: Not applicable; Flx Flexion, Ext Extension, LB Lateral bending, AR Axial rotation; P-A: Posterior-Anterior.

horizontal plane [59]. To assess detailed kinematics information in whiplash motion, the simulated head angle-time history curve was first compared with the PMHS experimental corridor [73]. Then, the head linear acceleration along horizontal sagittal motion, the horizontal/vertical sagittal displacements of the external auditory meatus (EAM), and the segment angular motions were also compared between the FE model and PHMS data. The criteria of Correlation and Analysis Rating (CORA) was adopted to evaluate the difference of two curves as the previous studies [32,33,74]. The CORA score ranges from 0% to 100%, while a higher score means better consistency of the compared curves.

2.3. Analysis of neural reflex influences

To investigate the influences of neural reflex control on head-neck biomechanical responses, the simulation results of two models were compared in a typical whiplash loading situation from the volunteer experiments of vehicle rear impact [75]. One is the present FE head-neck model without muscle activation. Another is the model with muscle activations derived from the neuromuscular model with vestibular and proprioceptive neural reflex control loops in OpenSim. The neuromuscular model was established by combining Python codes and OpenSim environment as reported in our recent study [34]. This combination method has been also previously adopted [29,76]. To reduce coupling heterogeneity, the initial parameters and position of the neuromuscular head-neck model were adjusted to be the same as the present FE head-neck model, including the head mass (4.5 kg), the distance from the skull to T1 (298 mm), and the neck length (128 mm). In both models, the skull center of gravity was located at rear edge of the sella turcica, and the Frankfort plane was defined to align with the horizontal plane.

The loading environment was following the experimental condition of Ono et al. [75] study. In this test, an impact velocity of 8 km/h was given to a rigid sled with a belted volunteer in the posterior-anterior direction. The PM-FEM and active muscles-FE model (AM-FEM) have the same passive muscle properties. Then, the latter obtained muscle activations from the neuromuscular model to produce active muscle forces. To verify model robustness and consistence of the two models, the head angle-time history curves of them were first compared with each other and the experimental corridor from seven volunteers. Then, vertical sagittal displacements and horizontal sagittal displacements of the occipital condyle (OC) were also analyzed as well as the segment angular motions. CORA was also adopted to evaluate the differences between two simulated curves. Finally, to explore the significance of neural reflex involvement in a whiplash loading condition, biomechanical responses of important adjacent tissues or segments were compared between the two models and the review of epidemiologic data on cervical spine injuries.

3. Results

3.1. Validation of the head-neck FE model

Anatomy measurements. The neck length that is the vertical distance from the spinous process of C7 to the tragus of the ear is 128.18 mm in the model, which is in the range of the measured data (122 ± 6 mm) by Vasavada et al. [63]. Vertebral height, depth, and width dimensions as well as the spinous process length of the model were all in good agreements with the experimentally measured ranges as shown in Fig. 2A.

Isolated tissues. In LCS and UCS ligaments' tension tests of the model, the force-displacement curves were within the experimental corridors concerning both curve shapes and peak failure values as shown in Fig. 2B. These simulation curves can be described as

an asymmetric sigmoidal shape up to the peak load, and exhibited typical regions of the toe, linear, and trauma in the process of tension. The range of ultimate load in LCS ligaments is about 75–500 N, while the UCS ligaments' range is about 75–1100 N, as shown in Fig. 2B(a) and 2B(b), respectively.

For the spinal cord, the simulated force-displacement curve of its dynamic indentation test lays in the range of the experimental corridor and shows a distinctive J-shaped curvature as the experimental data (Fig. 2C).

Segments. In the FSU compression, a reaction force of 744.18 N at 1.0 mm displacement is recorded, as shown in Fig. 2D. For the FSU rotation analysis, the full moment-rotation responses of the model are shown in Fig. 2E(a) and 2E(b). In flexion-extension loading condition, the range of motions (ROMs) of the separated and global FSUs are all within one standard deviation (SD) of the experimental data. As the experiments, the simulated ROMs of the UCS segment are higher than those of the LCS segment. In lateral bending, most of ROMs are in the experimental corridors except C4/5 and C6/7 segments. Their results fall out of the experiment corridor, but only present 1° difference from the SD. In terms of axial rotation, most segments scattered within the experimental corridors, excepting the relative movement of the C1-C2 that is at about 80% of the experimental average.

Anatomy measurements. A. Vertebral height, depth, and width dimensions as well as spinous process length of the model compared with the measured ranges.

Isolated tissues. B. Tension tests in all spinal ligaments of LCS (a) and UCS (b), where the respective force-displacement simulation curves were compared with the experimental data. C. Force-displacement curve of the spinal cord in comparison with the experimental corridor.

Segments. D. Force-displacement curve of the FSU in comparison with the experimental corridor. E. (a). Ramped steps of 0.5 Nm flexion-extension ROM for all segments. Vertical bars indicate SDs of the experimental data. (b). ROM at 1 Nm torque for lateral bending and axial rotation. Vertical bars indicate SDs of the experimental data.

Whole head-neck of PM-FEM. Compared with the PMHS responses reported by White et al. [73] study, overall trend of the simulated head angle-time history curve is well correlated with the experimental corridor (Fig. 3). The CORA score between the simulated curve and the center line of the experimental corridor reaches 88.7%. The simulated peak angle is 90.74° at 216 ms. From the toe region to the initial linear region, the simulated curve is not totally in the corridor. The earlier incline process can be attributed to the lack of the skin, fat, thyroid, trachea, and esophagus in the model that was also previously discussed [24]. In addition, the other biomechanical responses of the model including the head linear acceleration along horizontal motion, the vertical/ horizontal sagittal displacements of EAM, and the segment angular motions, were all well correlated with the experimental results as shown in Appendix Fig. 1.

3.2. Analysis of neural reflex influences and its comparison with epidemiologic data

During the combined simulation, muscle activation levels of 12 muscles were first extracted from the neuromuscular model simulation with vestibular and proprioceptive reflex controls (Fig. 4A-B). Then, these activation levels were input to the present head-neck FE model for tissue injury risk analysis (Fig. 4C). The kinematic responses of both the neuromuscular and present FE models were in good agreements with the experimental corridor (Fig. 4D). The CORA score of two simulated curves reaches 90.7%, which indicates a good match. The unavoidable difference can be attributed to the model difference in structure and solution theory. For example, the

intervertebral discs and ligaments are not included in the musculoskeletal model but fully modeled in the FE model.

The comparison of head-neck kinematic responses between the AM-FEM and the PM-FEM was shown in Fig. 5. Before 125 ms, the head rotation angles of the two models are similar. After that, a substantial deviation appears and gradually increases. The peak rotation angle of the AM-FEM at 225 ms is about half of the PM-FEM model. This indicates that the muscle activation induced by

the neural reflex can significantly limit head-neck rotation. Alike findings can be also noted in the comparison of vertical/horizontal sagittal displacements (OC) and segment angular motions in Appendix Fig. 2. It also means that the neural reflex can large reduce head-neck injury risk during whiplash loading condition.

Peak stress/strain distributions and their corresponding loading times for spine bone and ligament structures are shown in Fig. 6 and Fig. 7. With regard to spinal ligaments, the UCS ligaments

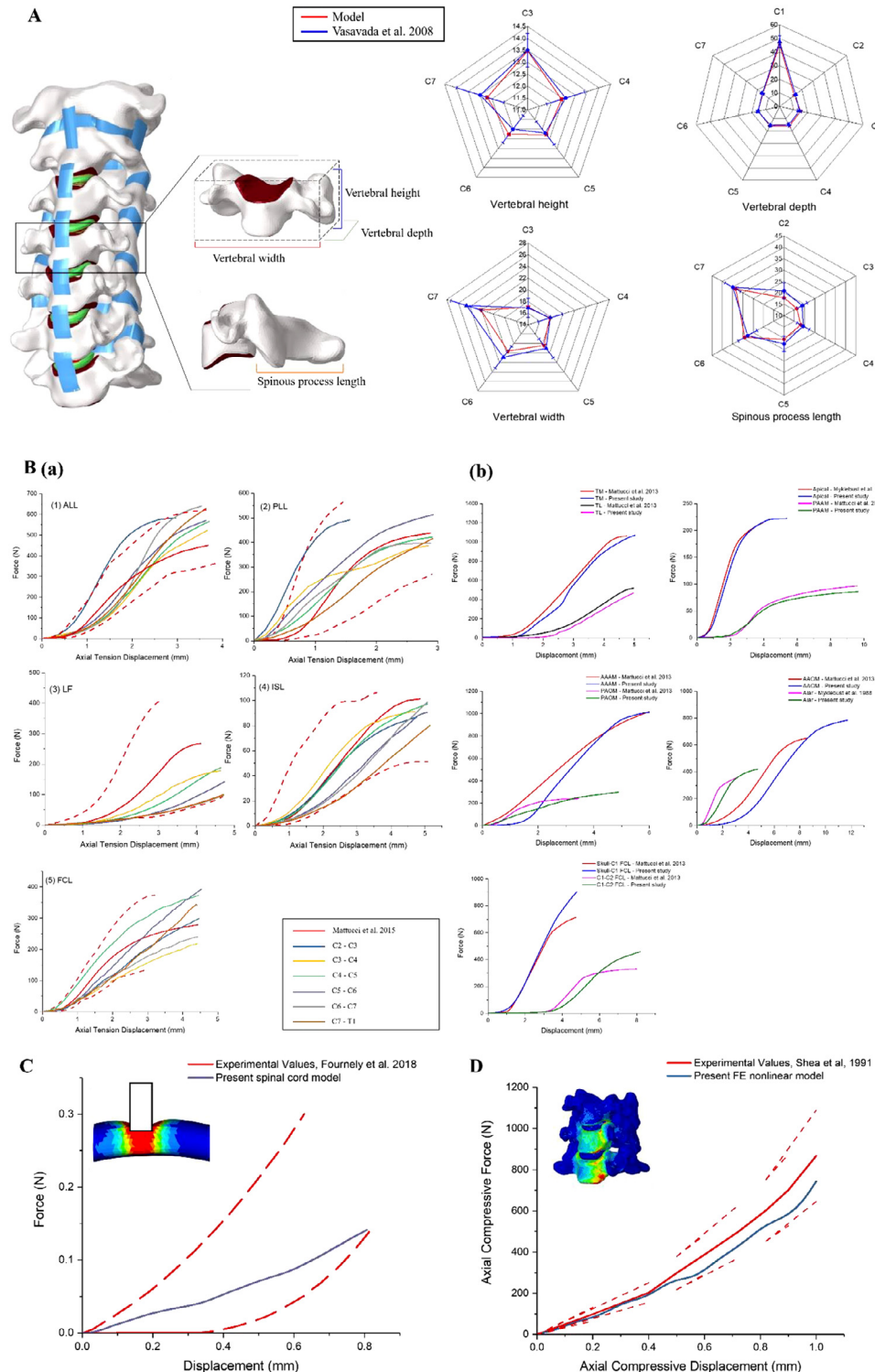


Fig. 2. Views of multilevel validation of the FE head-neck model.

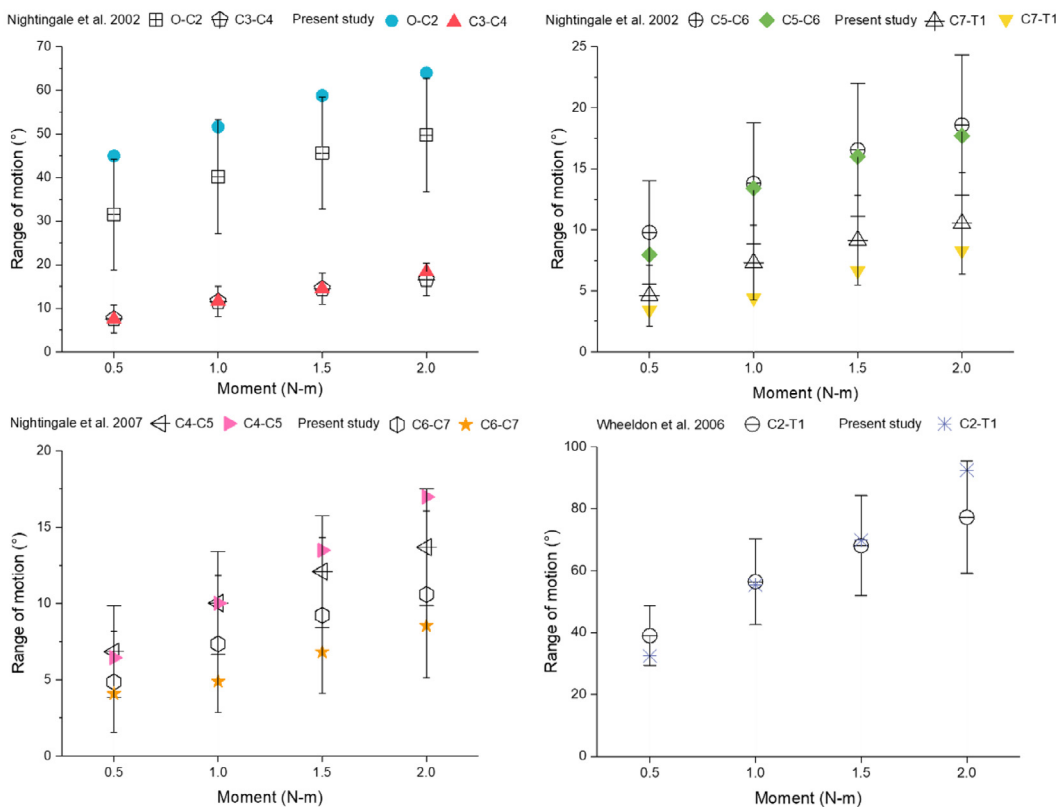
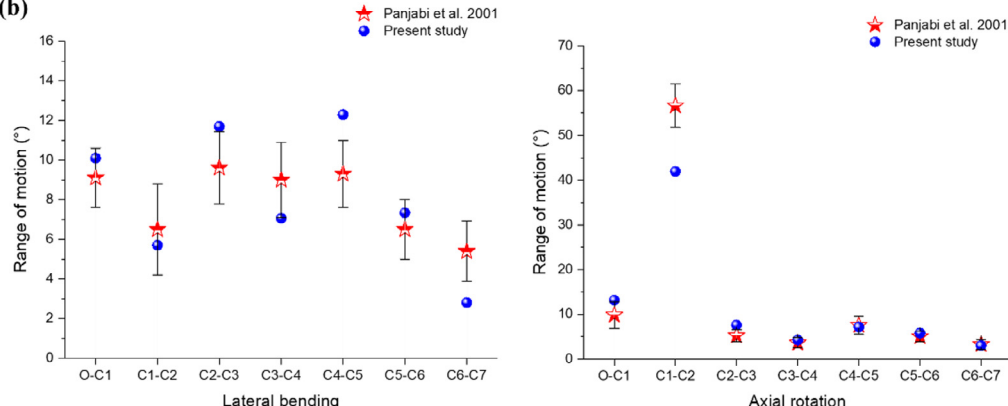
E (a)**(b)****Fig. 2. Continued**

Table 3
Incidences of trauma cervical-disk levels in whiplash injury of real-world outcomes.

Studies	Trauma incidences (%) of disk levels				
	C2/3	C3/4	C4/5	C5/6	C6/7
Davis, et al. 1991 ($n = 13$)		7.7	7.7	53.8	30.8
Jónsson, et al. 1991 ($n = 26$)	19.2	15.4	26.9	26.9	11.6
Hamer, et al. 1993 ($n = 35$)		5.7	20	45.7	28.6
Pettersson, et al. 1994 ($n = 40$)	2.5	10.0	35.0	42.5	10.0
Jónsson, et al. 1994 ($n = 22$)		4.6	4.6	72.7	18.1
Stäbler, et al. 2001 ($n = 8$)	50.0	50.0			
Kongsted, et al. 2008 ($n = 10$)	20.0	10.0	50.0	20.0	

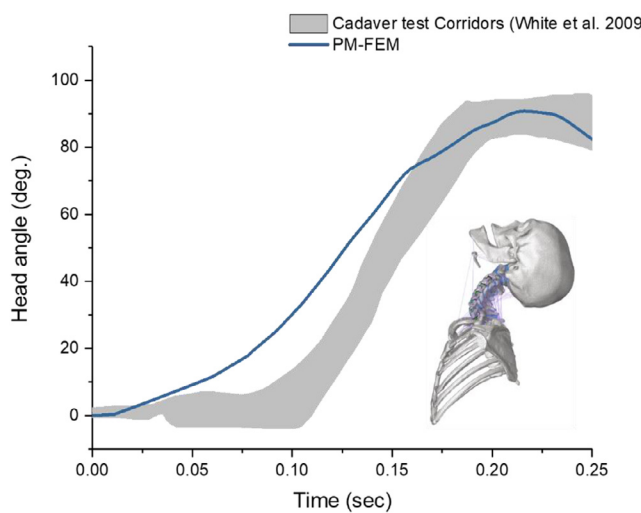


Fig. 3. Global kinematics of the head angle-time history compared with the PMHS corridor in 4 g rear impact for validating the whole head-neck model.

of the PM-FEM model are obviously larger than those of the AM-FEM model as shown in Fig. 6A. Among them, the peak strain of the skull FCL in the PM-FEM model is two times larger than that of the AM-FEM one. The LCS ligament strain levels of the PM-FEM are also larger than those of the AM-FEM. The difference is in the range of 0.6% to 14.5% (Fig. 6B).

For bony structures (Fig. 7), overall stress level of the PM-FEM is larger than the AM-FEM. The peak Von Mises stress of the PM-FEM occurred in the C6 spinous process, and presents a high stress level from C2 to C6, while the AM-FEM shows a high stress level from C4 to C6, which is only about 25% of the PM-FEM peak value. Most vertebrae stress values of the AM-FEM are below 0.1 GPa together with being more evenly distributed.

The peak stress levels of the AM-FEM vertebra-discs are generally lower than those of the PM-FEM except for C4/5 and C5/6 discs. Compare with the PM-FEM, the AM-FEM presents higher stress levels in these two discs (Fig. 8). Only the peak stresses of C4/5 and C5/6 discs are larger in the AM-FEM. An obvious feature

is that the large stresses of the AM-FEM discs are primarily concentrated in the C4-C6 region. But for the PM-FEM, they disperse in the discs from C2-C6.

For the spinal cord, overall strain levels of the AM-FEM are obviously lower than the PM-FEM in both GM and WM (Fig. 10A). The spinal cord region of the maximum strain also shows a variance due to the intervention of neural reflex. The AM-FEM indicates that spinal cord injury (SCI) risk concentrated near C4 segment, while the PM-FEM indicates around C1 segment. Besides, the morphology of spinal cord model in the AM-FEM is much less distorted, and only about 1/3 of GM's peak strain and 1/2 of WM's peak strain of the PM-FEM (Fig. 10A). The stress level showed a similar trend as the strain level, while the peak Von mises stress of the AM-FEM is about only 1/10 of the PM-FEM (Appendix Fig. 3).

Although these epidemiological studies do not provide detailed trauma levels in damage incidents, similar type of hyperextension injury (sudden acceleration-deceleration injured mechanism) occurred compared with whiplash. In addition, epidemiological data about SCI of isolated whiplash injury are few [77–79], worldwide epidemiological studies about trauma SCI included whiplash injury were reviewed, which belongs to a kind of injury load in cervical spine. Fourteen studies [80–93] from 1985 to the present showed that C4 to C5 segments sustained most trauma incidences at spinal cord level in real-world accidents, as shown in Fig. 11 and Table 4. Some of the researches included statistics data on whiplash injury [81,83,91]. The injury percentages are 8.7%–52.0% for C4 segment and 15.2%–53.6% for C5 segment. Two studies even reported that the incidence can be up to 60.8%–66.3% of both segments. Some clinical studies also revealed that C4 to C5 segments sustained most injuries in SCI of cervical hyperextension trauma [94–96].

4. Discussion

Based on the development and validation of a new head-neck FE model with active muscles and spinal cord modeling, the present study simulated an in-vivo response of human head-neck system by considering vestibular and proprioceptive reflex loops, and analyzed the effects of neural reflex on neck kinematics that would have implications on injury risk in a typical loading condition (whiplash). Due to muscle activation forces caused by neu-

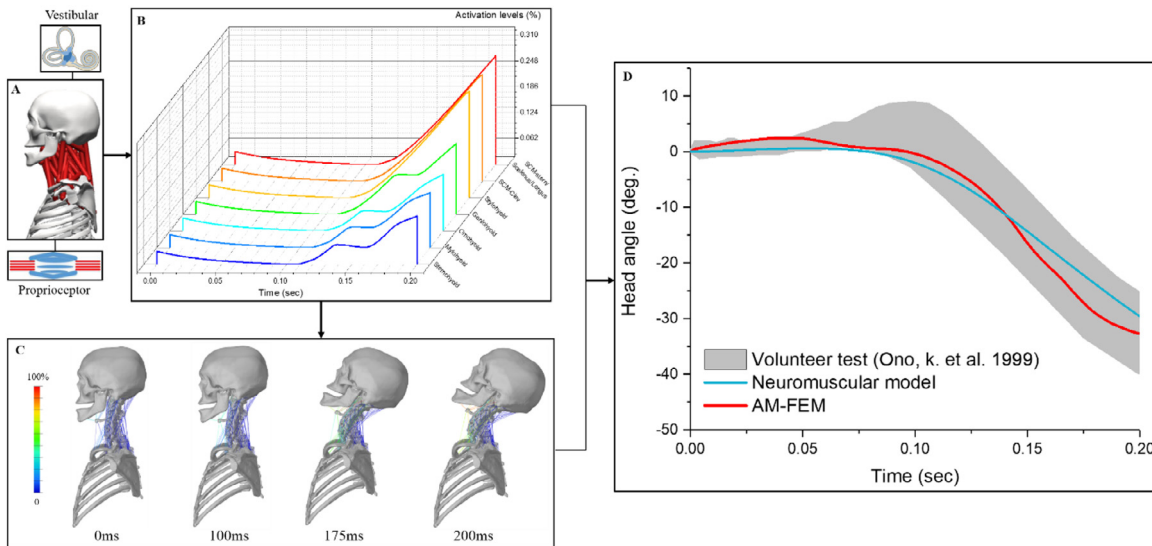


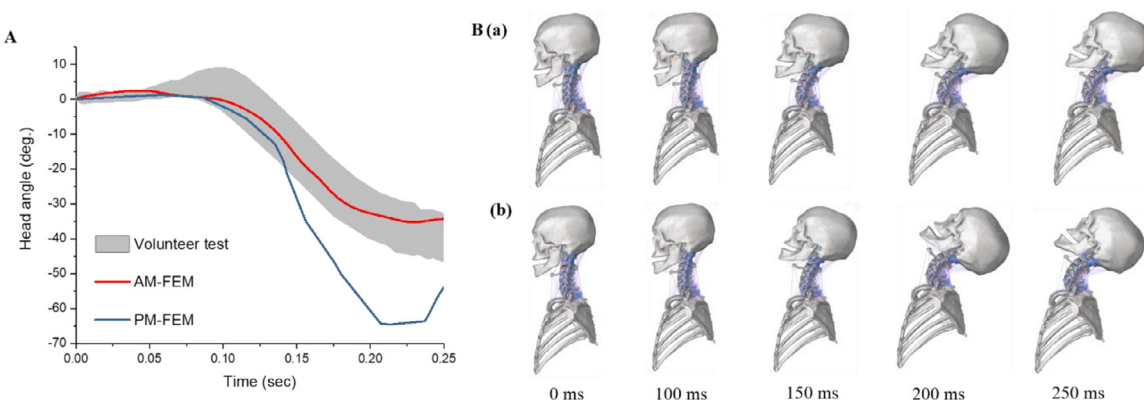
Fig. 4. A. A specific neuromuscular head-neck model with crucial neural control factors including vestibular and proprioceptive reflex loops. B. Muscle activation levels extracted from the neuromuscular model simulation. C. A FE simulation coupling with the neuromuscular model by imposing multiple muscle activation curves. D. Comparison of head-neck kinematics between the musculoskeletal analysis and the FE simulation.

Table 4

Incidences of trauma spinal levels in SCI of real-world outcomes.

Studies	Types	SCI Incidences (%) of spinal levels						
		C1	C2	C3	C4	C5	C6	C7
Burke, et al. 1985 (n = 168)	Road accident (52.0%); Sport (16.0%); Domestic (12.0%); Occupational (10.5%); Other (7.7%); Framing (1.8%)	19.6			60.8		19.6	
Yoganandan, et al. 1989 (n = 103)	Compression-flexion (46.6%); Burst (13.6%); Extension (6.8%);	1.0	10.7	4.9	9.7	30.1	35.0	8.7
	Road accident Flexion-rotation (14.6%); Flexion (6.8%); Locked facets (10.7%); Unknown (1.0%)							
Go, et al. 1995 (n = N/A)	N/A				22.0	46.0	11.0	
Koyanagi, et al. 2000 (n = 42)	Fall to ground (50%); Traffic accidents (29%)		40.0	37.0	21.0	2.0		
O'Connor, 2002 (n = 150)	Fall from height (17%); Others (4%)							
	Transport related injury (43%); Sport (5%); Others (52%)	6.7	6.0	31.3	29.3	16.7	10.0	
O'Connor, et al. 2006 (n = 23)	Motor vehicle collisions (50.0%); Falls (37.0%); Sport (9.0%); Clinical procedure (4.0%)	4.3	17.4	30.4	39.1	4.4	4.4	
Ye, et al. 2009 (n = 50)	Sport (64.9%); Others (35.1%)	2.0	2.0	4.0	52.0	18.0	14.0	8.0
Ning, et al. 2011 (n = 617)	Fall (56.9%); Struck (6.3%); Motor vehicle collision (34.1%)	1.3	3.9	25.1	53.6	12.2	3.9	
Wu, et al. 2012 (n = 142)	Fall (49.7%); Motor vehicle collision (36.4%); Sport (4.2%); Work accident (3.2%); Assault (1.4%); Others (1.4%)	3.5	2.8	15.5	43.0	26.8	8.4	
Zhou, et al. 2016 (n = 240)	Fall (55.1%); Motor vehicle collision (35.9%); Sport and Struck (2.8%); Others (6.2%)	5.4	3.0	17.5	53.3	17.9	2.9	
Ning, et al. 2016 (n = 302)	Fall (61.7%); Motor vehicle collision (21.8%); Struck (13.8%); Others (2.7%)	12.9	16.5	20.0	29.7	17.8	3.1	
2016 Annual Report-National SCI Statistical Center (U.S.) (n = 30,393. 45.5% SCI)	Auto accidents (32.5%); Fall (22.2%); Gunshot wounds (15.3%); Sport (14.1%); Motorcycle accidents (6.1%); Others (4.2%); Hit by objects (2.8%); Medical complications (2.8%)			15.0	15.2	10.2	5.1	
Montoto-Marqués, et al. 2017 (n = 630)	Fall (54.2%); Traffic accidents (37.0%); Sports (3.5%); Others (5.3%)	13.3		66.3		20.4		
Krappinger, et al. 2019 (n = 23)	Hyperextension injuries		34.8	8.7	47.8	8.7		

N/A: Not applicable.

**Fig. 5.** A. Comparison of head-neck kinematics. B. Comparison of respective working conditions between the AM-FEM (a) and PM-FEM (b).

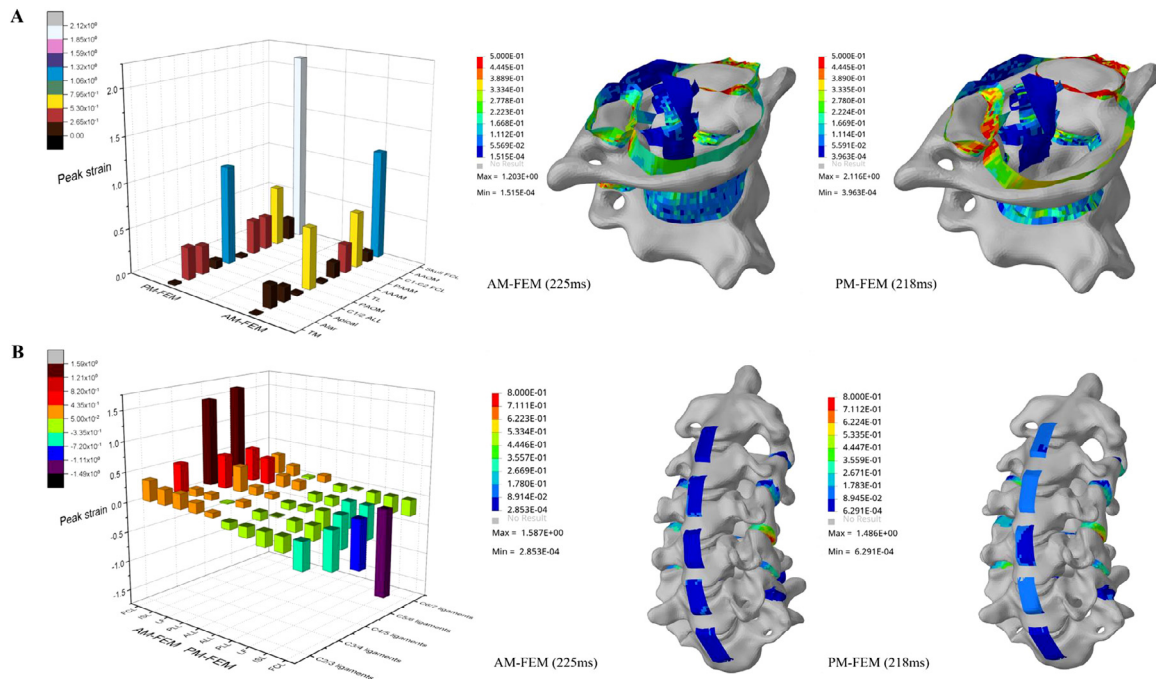


Fig. 6. A. Comparison of peak strain and strain distribution nephograms in the UCS ligaments. B. Comparison of peak strain and strain distribution nephograms in the LCS ligaments.

ral reflex, head rotation angles, tissue strain and stress levels as well as load concentration locations were largely changed. When comparing to volunteer experiments and epidemiological studies, the active head-neck FE model with neural reflex effects can better simulate *in vivo* responses and identify potential injury risk and locations. As shown in Fig 5, the AM-FEM shows a normal head-neck rotation angle in the experimental corridor, but the head-neck rotation angle of the PM-FEM (63.5°) in this simulation exceeds the range of physiological motion (51.3°) from the report of intervertebral neck injury criterion by Panjabi et al. [97].

Regarding the spinal cord, the two models show substantial differences concerning both peak strain values and locations (Fig. 10). In this whiplash loading simulation, the PM-FEM displayed the highest strain level in C1 area. But injuries to the spinal cord at C1 or C2 levels were rare, extremely severe, and most often fatal in real accidents. The AM-FEM showed the largest strain values around C4 segment, while the previous epidemiological data also showed that the most common injury levels are around C4 to C5 (Fig. 10–11 and Table 4). The previous studies indicated a possible reason that the C4/C5 FSU is the apex of the physiological lordosis, and the relative narrowing of the canal occurs at C4 to C5 [98,99]. Panjabi et al. proposed a well-known hypothesis of the spine stabilizing system, which indicated that the function of neural element regulates muscles to protect the spine [1,4]. Clinical studies also indicated a possible role of awareness in injury outcome [100,101]. Here, our simulation results verified the hypothesis and further quantitatively indicated that the muscle activation caused by neural reflex is providing a protection in impact loading by reducing strain/stress levels and changing possible injury to lower spinal cord level.

For intervertebral discs, the AM-FEM shows a concentrated stress region at C4/5 and C5/6, which accords with epidemiological statistics of high-risk disk damage region in whiplash injury (Fig. 8–9). C4/C5 is typically more mobile compared to other motion segments as previously reported [102]. Our simulation results indicated another possibility. The lateral anterior bundles of longus capitis and longus colli intensively originate from the transverse

processes of C4 to C6. In the simulation, the active force from the longus capitis and longus colli aggravated the compression of adjacent vertebrae-intervertebral discs in the model. Subsequently, the AM-FEM produced larger peak stress values than the PM-FEM at C4/C5 and C5/C6 discs, but far lower stresses at C2/C3 and C3/C4 discs (Fig. 8). The PM-FEM without active muscle forces conducted a high stress concentration in discs with similar peak values from C2 to C6. For bony structures and ligaments, the AM-FEM model generally showed lower peak stress and strain values compared with the PM-FEM. The PM-FEM even produced an abnormal avulsion fracture that cannot happen in a volunteer experiment. Since the model lacked the protection of soft tissues surrounding the bony structure, the stress on the bony structures can be greater than reality. The reduced ligament loads in the AM-FEM could potentially protect from a rupture as ligaments primarily are in tension loading.

Kreipke et al. [78], Rizzolo et al. [79], and Evans [103] argued that vertebral fractures and dislocations were rare in whiplash injury. Few radiographic studies reported that potential injury could occur in the bony endplate, lamina, and spinous process, which was concentrated in C5 to C7 region [104–106]. However, Griffiths et al. reviewed these studies and claimed that most of these patients had injuries more severe than those seen with a typical whiplash injury [107]. Such studies recorded scattered data and were primarily presented in case reports, which was hard to form a series of clinical studies. But limited data was also well correlated with stress concentrated locations of the AM-FEM simulation results.

More clinical studies focused on intervertebral disk lesion in whiplash injury, which plays an important role in following chronic pain. Seven studies [104,106,108–111] from the past thirty decades indicated that C4/5 and C5/6 discs typically sustained most trauma incidences compared to other motion segments in whiplash injury (Fig. 9 and Table 3). Median incidences are 22.0% of C4/5 and 48.6% of C5/6 disk. The previous reviews indicated that the strains are largest in C4/5 disk at low accelerations [112,113]. These locations are in

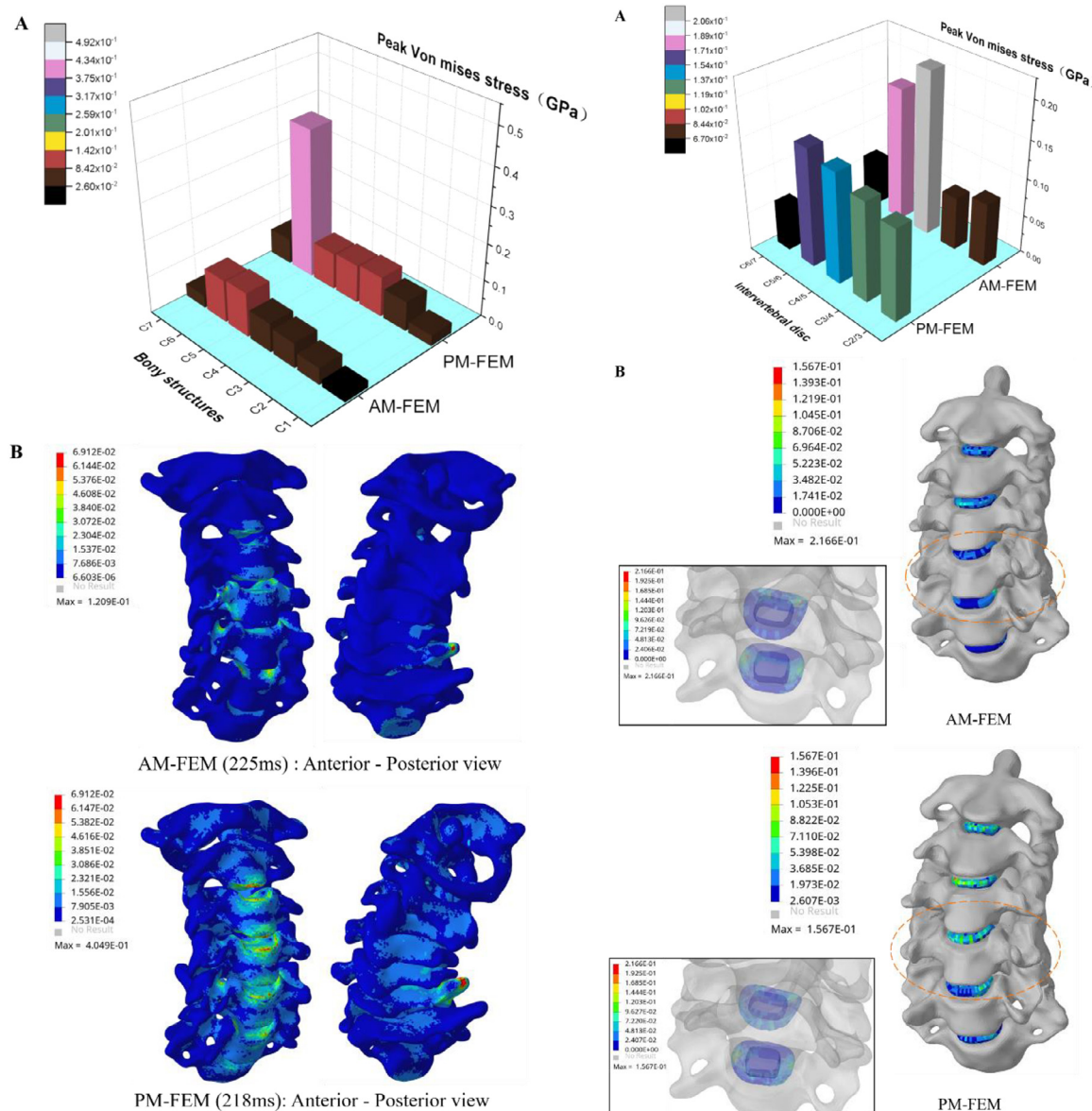


Fig. 7. A. Comparison of peak Von mises stress in bony structures. B. Stress distribution nephograms of the vertebrae in both groups.

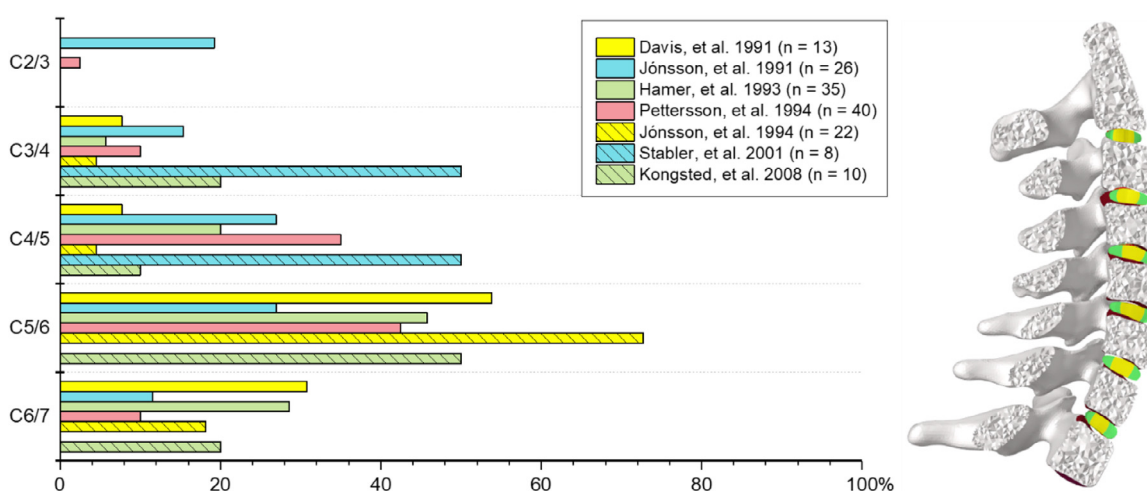


Fig. 8. A. Comparison of peak Von mises stress in intervertebral discs. B. Stress distribution nephograms of the intervertebral discs in both groups.

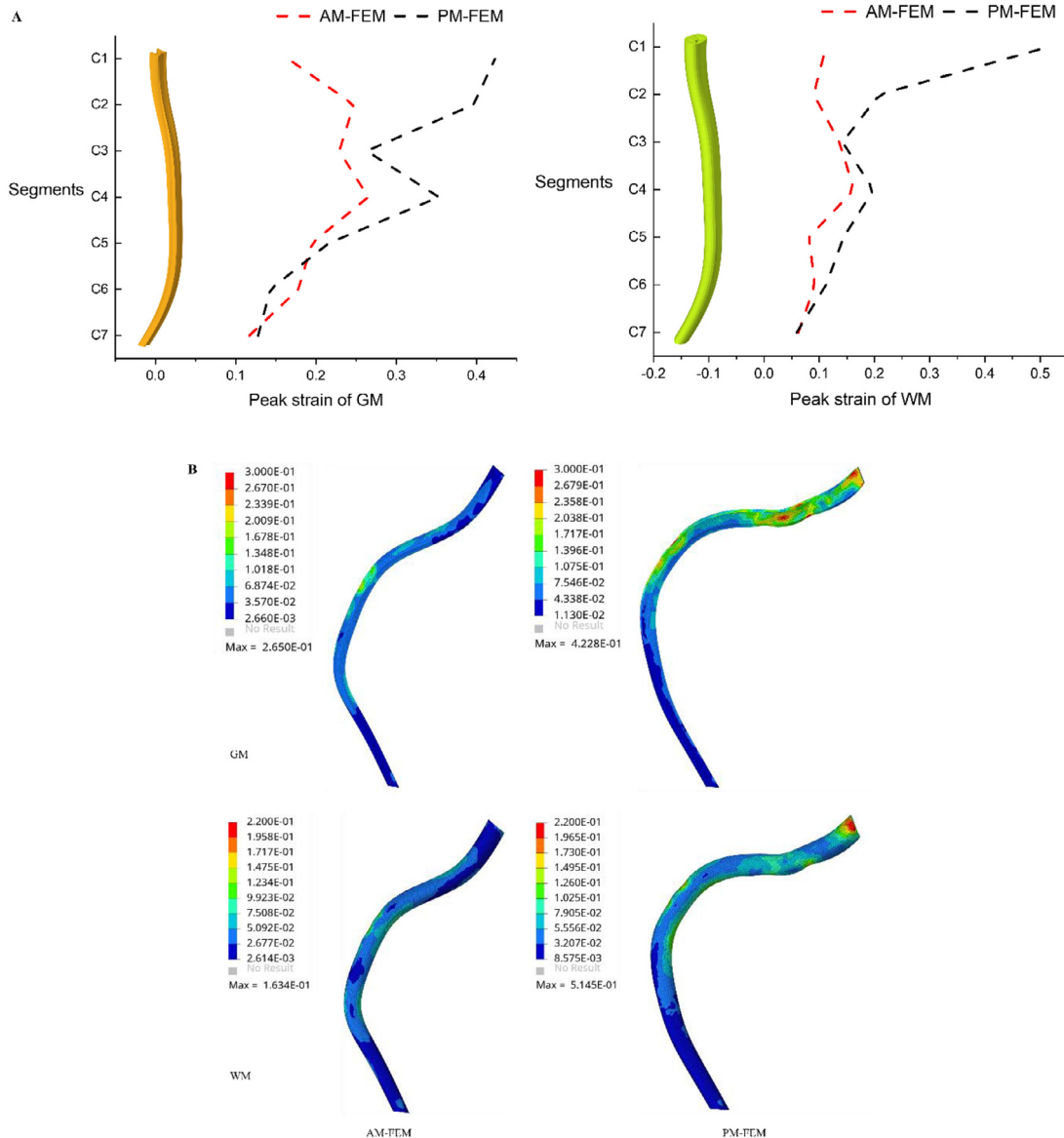


Fig. 9. Incidences of trauma cervical-disk levels in whiplash injury of real-world outcomes.

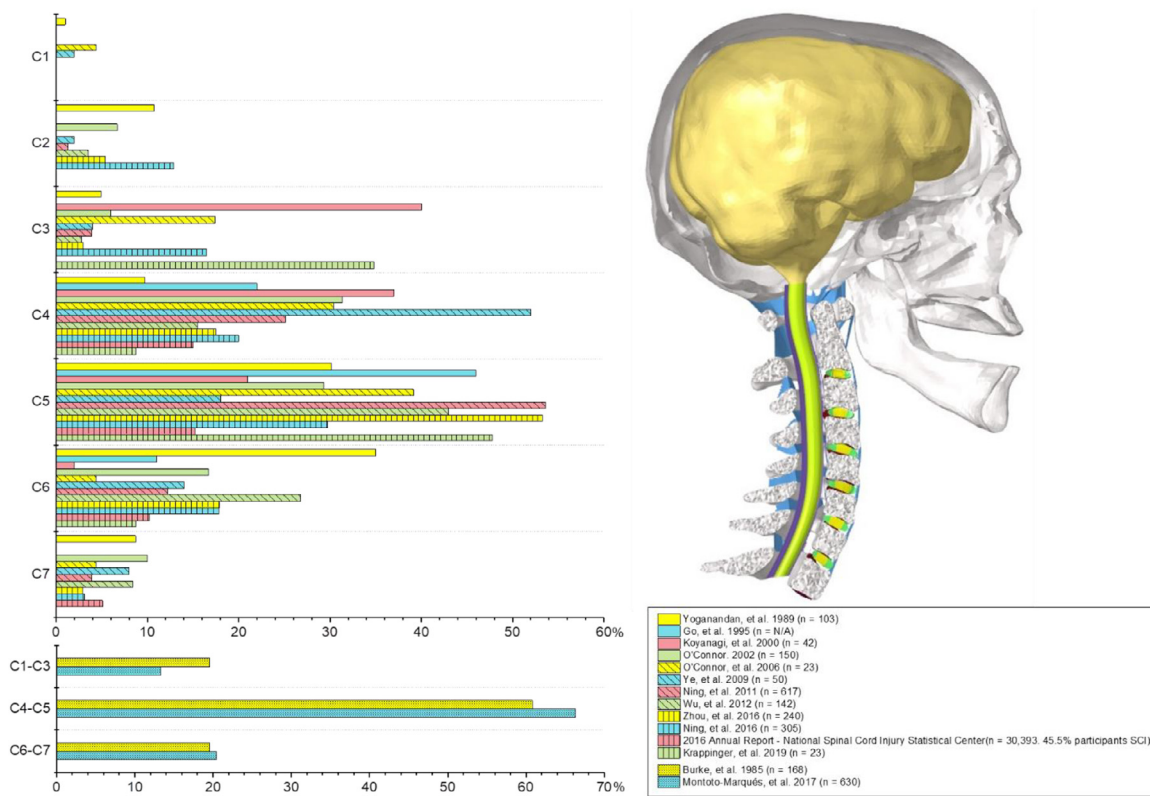


Fig. 10. A. Strain distribution nephograms of the GM and WM in both groups. B. Peak strain comparison of GM and WM area in each cervical spine segment.

good agreements with the injury risk findings of the AM-FEM simulation.

The above analysis demonstrated our model biofidelity and the necessity of considering the neural reflex in the FE model to achieve an accurate analysis of the head-neck motion and internal loading. There are still limitations or future extension studies can be implemented. First, the coupling method of musculoskeletal and FE models was efficient and largely used in the previous studies [29,76,114], but unavoidable differences always existed between these two model types that can be primarily attributed to solution theory difference. For example, the intervertebral discs and ligaments are not included in the musculoskeletal model but fully modeled in the FE model. Further improvement for the musculoskeletal model can be implemented to achieve a better match. Some recent studies included pre-defined activation-time curve [18,19,24,25], PID [26,115] and other artificial control methods to represent neural control in FE models [28,31,32,34]. In our previous trials [30], the computational cost is huge especially when the modeling complexity of the neural control method is increased to be humanlike. The present method of coupling musculoskeletal model and FE model can save the huge computational cost for better engineering application. Second, the head rotation angle curve of our passive FE model in whiplash loading showed an earlier incline as the previous study [24]. This is partly due to the current lack of soft tissue representation. If the neck model would have the surrounding soft tissue represented, it would be possible to obtain the same maximum angular head displacement but with largely reduced neck stiffness. In such a case, the neck would be less prone to follow the upper body movement and would thus not be forcefully pulled forward at the time that the upper body moved forward. The current neck model resulted in a rapid response (the earlier incline process) similar to what was discussed in previous research [116]. Another reason can be similar to the difference that appeared between the Hybrid III dummy and the

BioRID II dummy. The previous studies indicated that the BioRID II dummy fitted with a softer thoracic spine in order to allow a larger T1 upward motion [117], when compared with the high stiffness thoracic spine of the Hybrid III dummy [118]. In the present study, the thoracic spine was set to be rigid and the T1 vertebra loading conditions was simplified to be only accelerating in the horizontal forward direction. We believe that all these are primary reasons of the earlier incline process. Thus, modeling details can be further improved in the future. Third, the present study validated and analyzed model biomechanical responses through the volunteer experiments that generally would not include injury occurrences, in order to including natural human reflex responses. Then, the stress and strain levels were used to evaluate possible injury risk. In the future, more serious loading conditions that can cause substantial neck injuries can be further explored. Finally, spinal cord was included in the present FEM for rear impact analysis as whiplash injury probably cause compression on the nerve roots due to the pressure transient in the central nervous system [119,120]. Some studies revealed that lesions of spinal ligaments, other membranes, and intervertebral discs could be injured during a whiplash motion [121–126]. Anatomically, these tissues are very close to the spinal canal. Beausejour et al [123] indicated SCI can be aggravated due to the extent of posterior disco-ligamentous injury and joint instabilities. To our knowledge, spinal cord was not included in many previous models [19,21,22,59,127–129]. In the present model, this item was modeled using a hyper-elastic Ogden material model based on the recent experimental studies of in vivo non-human primates. The contact setting of the components in cervical vertebral canal also allows for axial motion in this model, which is consistent with physiological sagittal motion of intraspinal tissues [130]. However, the model still lacks the detailed modeling in spinal canal, such as venous network, arterial network, and CSF system, like the previous model of Yao et al. study [131]. Synchronized interaction between fluid (blood vessel, CSF)

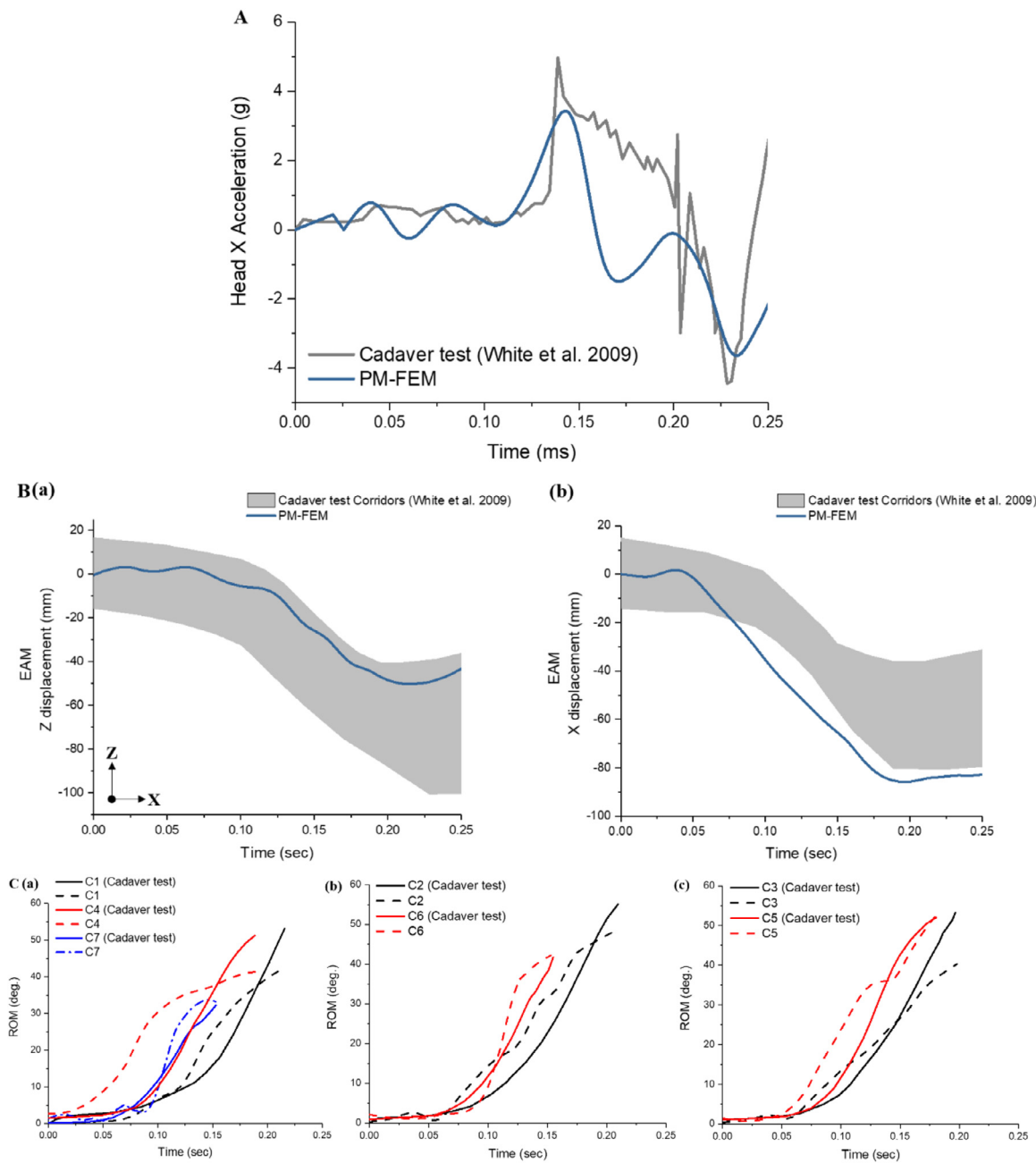


Fig. 11. Incidences of trauma spinal levels in SCI of real-world outcomes.

and structure (spinal cord) is neglected. This interaction of pulling and pressing processes may increase tension in the spinal cord leading to the WADs [132]. Neglecting these effects is a simplification of the present work, which should be the improving direction of our model. In addition, more experimental studies on spinal cords can be needed in the future for more accurate FE modeling.

5. Conclusion

The present study established and validated an active FE head-neck model at multi-levels, and demonstrated an important role of neural reflex control in limiting head rotation and neck injury risk. The obvious simulation differences indicated that integrating neural reflex effects should be necessary to accurately predict head-neck biomechanical responses using numerical method. The present method can be one way for future FE analysis of head-neck system in various applications. Focusing on a typical spinal injury loading condition (whiplash), tissue load concentration locations as well as stress/strain levels of the head-neck system were both changed due to the muscle activation forces caused by neural reflex control during the whole loading process. For most tissues or segments, peak stress or strain levels were significantly reduced

as the muscles activated by neural reflex signals limited the head-neck rotation. It was worthy of noting that the strain/stress concentrated locations were evidently transferred to a lower cervical spine region when these muscles were activated by neural reflex control.

Declaration of Competing Interest

The authors declared no potential conflicts of interest with respect to the research, authorship, and/or publication of this article.

Acknowledgments

This work is supported by the National Natural Science Foundation of China (Grant No. 51875187), Hunan Youth Talent Program (Grant No. 2020RC3016), and Key Research and Development Program of Hunan Province of China (Grant No. 2022SK2105).

Appendix

Table A1 and Fig. A1, A2, A3.

Table A1
Definition of muscle properties.

Musculus flexors	PCSA(mm ²)	F _{max} (N)	Musculus extensors	PCSA(mm ²)	F _{max} (N)
Sternocleidomastoid-stern	70	35	Trapezius	256	128
Sternocleidomastoid-clav	48	24	Rhomboideus minor	48	24
Scalenus-Post	44	22	Serratus posterior superior	26	13
Scalenus-Med	26	13	Levator scapulae	40	20
Scalenus-Ant	20	10	Rectus capitis posterior minor	90	45
Longus capitis	22	11	Rectus capitis posterior major	54	27
Longus colli	12	6	Obliquus capitis superior	92	46
Geniohyoid	97	34	Obliquus capitis inferior	172	86
Mylohyoid	160	56	Interspinales cervicis	12	6
Omohyoid	74	26	Semispinalis cervicis	44	22
Sternohyoid	57	20	Multifidus	34	17
Stylohyoid	20	7	Splenius capitis	18	9
Rectus capitis lateralis	78	39	Semispinalis capitis	34	17
Rectus capitis anterior	8	4	Longissimus capitis	12	6
InTrans Anterior Cervicis	8	4	Longissimus cervicis	16	8
InTrans Posterior Cervicis	16	8	Iliocostalis cervicis	14	7

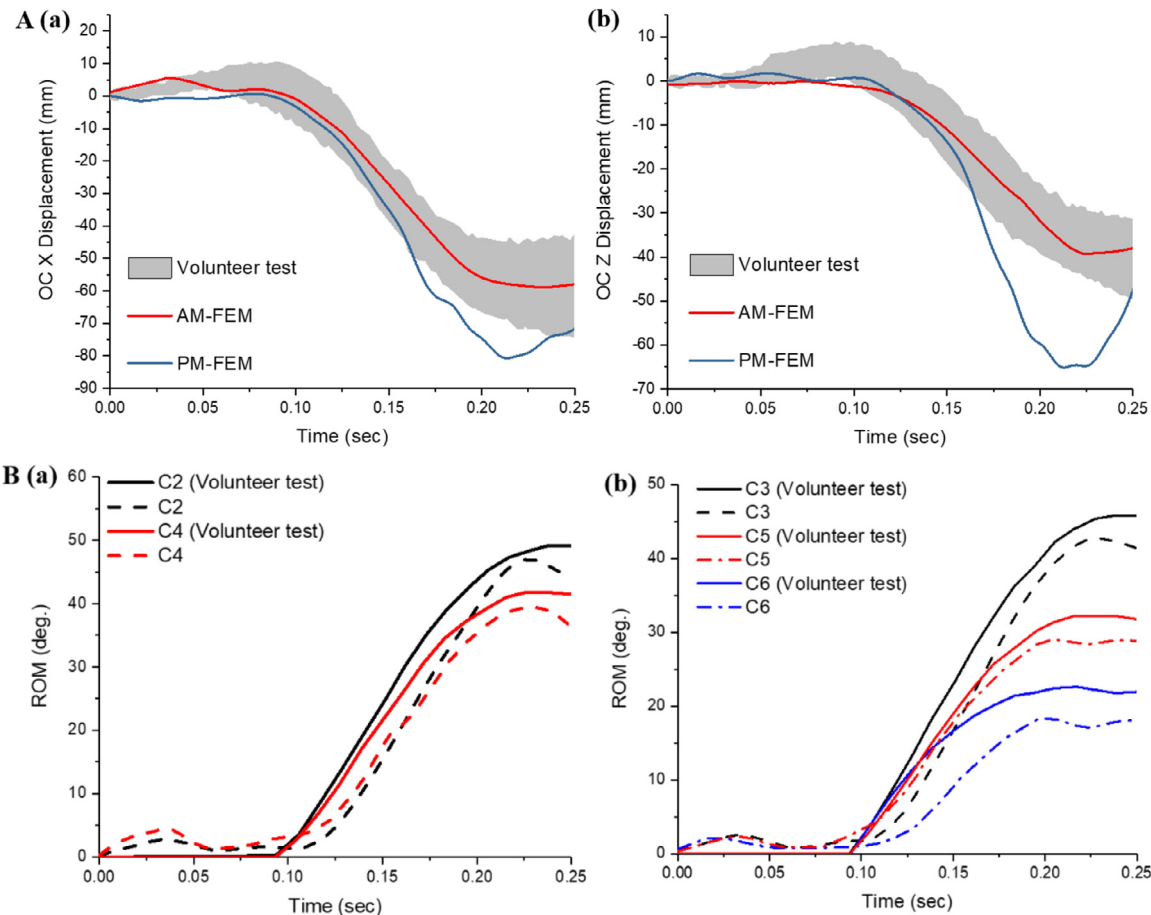


Fig. A1. A. Comparison of head linear acceleration along horizontal sagittal motion (X-axis) between the PM-FEM simulation results and PHMS data; B (a, b). Vertical sagittal displacements (Z-axis) and horizontal sagittal displacements (X-axis) of EAM between the PM-FEM simulation results and PHMS data (CORA score 80.2% and 66.3%, respectively); C (a-c). Comparison of segment angular motions between the PM-FEM results and PMHS data.

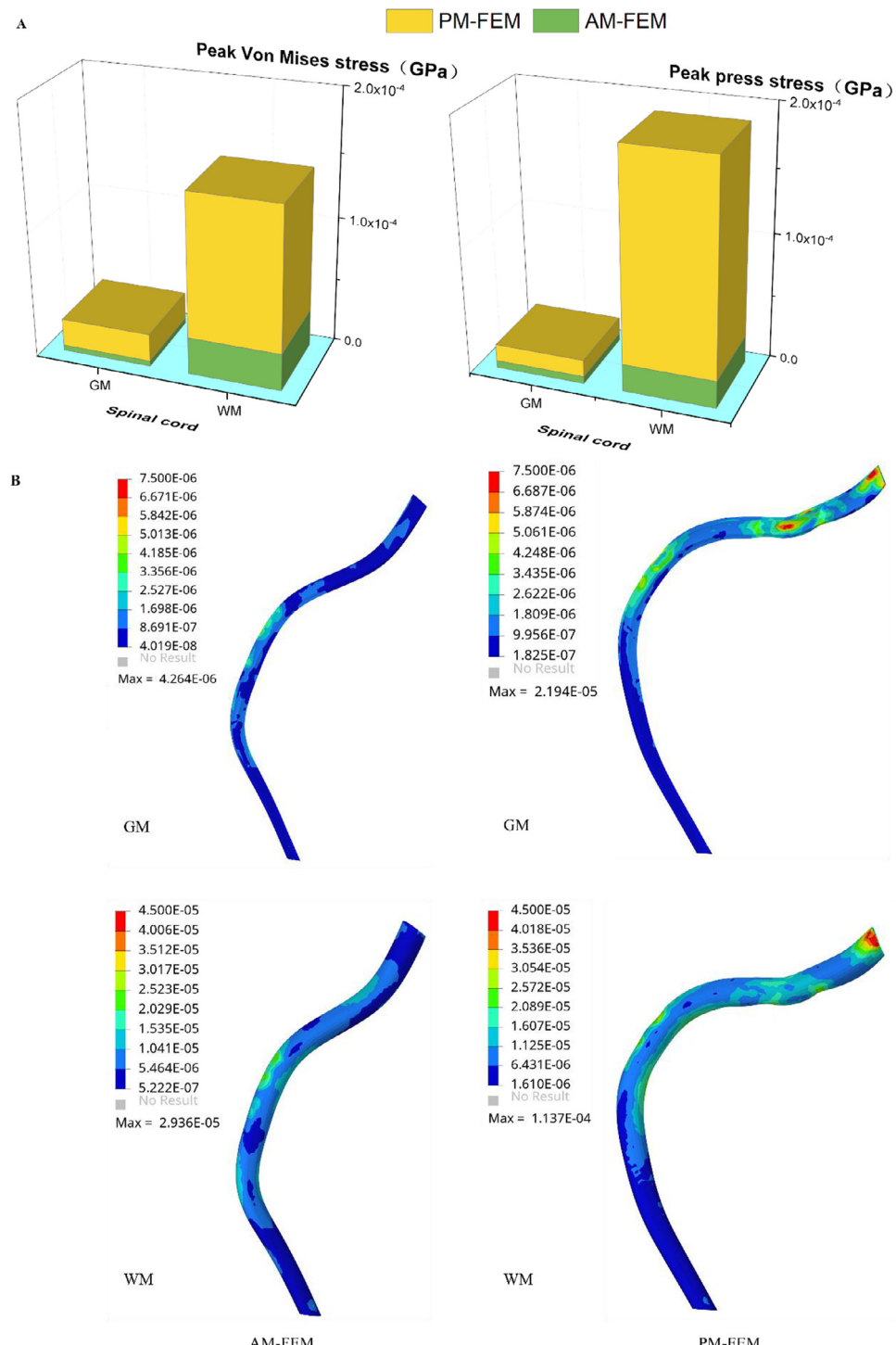


Fig. A2. A (a, b). Horizontal sagittal displacements (X-axis) and vertical sagittal displacements (Z-axis) of OC between FE models and volunteer data (For the AM-FEM model, CORA score 94.2% and 88.0%, respectively); B (a, b). Comparison of segment angular motions between the AM-FEM model and volunteer data.

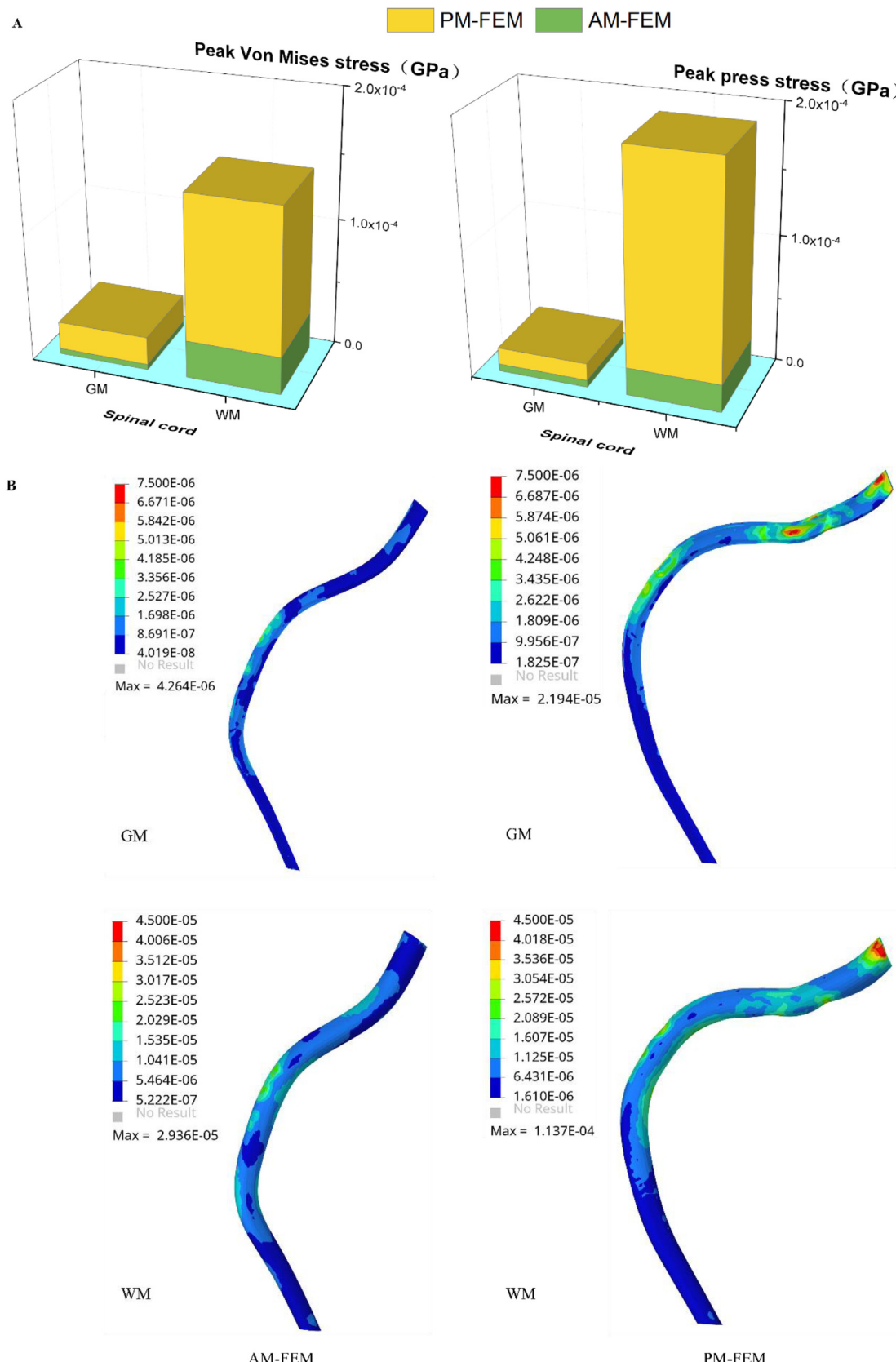


Fig. A3. A. Comparison of peak Von mises stress and peak press stress in the spinal cord area. B. Von mises stress distribution nephograms of the GM and WM in both groups.

References

- [1] M.M. Panjabi, The stabilizing system of the spine. Part I. Function, dysfunction, adaptation, and enhancement, *J. Spinal Disord.* 5 (1992) 383–389 discussion 397, doi:[10.1097/00002517-199212000-00001](https://doi.org/10.1097/00002517-199212000-00001).
- [2] M. Solomonow, B.H. Zhou, M. Harris, Y. Lu, R.V. Baratta, The ligamento-muscular stabilizing system of the spine, *Spine (Phila Pa 1976)* 23 (1998) 2552–2562, doi:[10.1097/00007632-199812010-00010](https://doi.org/10.1097/00007632-199812010-00010).
- [3] J. Hoffman, P. Gabel, Expanding Panjabi's stability model to express movement: a theoretical model, *Med. Hypotheses* 80 (2013) 692–697, doi:[10.1016/j.mehy.2013.02.006](https://doi.org/10.1016/j.mehy.2013.02.006).
- [4] M.M. Panjabi, The stabilizing system of the spine. Part II. Neutral zone and instability hypothesis, *J. Spinal Disord.* 5 (1992) 390–396 discussion 397, doi:[10.1097/00002517-199212000-00002](https://doi.org/10.1097/00002517-199212000-00002).
- [5] P.W. Hodges, C.A. Richardson, Contraction of the abdominal muscles associated with movement of the lower limb, *Phys. Ther.* 77 (1997) 132–142 discussion 142–134, doi:[10.1093/ptj/77.2.132](https://doi.org/10.1093/ptj/77.2.132).
- [6] G.L. Moseley, P.W. Hodges, S.C. Gandevia, External perturbation of the trunk in standing humans differentially activates components of the medial back muscles, *J. Physiol.* 547 (2003) 581–587, doi:[10.1113/jphysiol.2002.024950](https://doi.org/10.1113/jphysiol.2002.024950).
- [7] P.W. Hodges, C.A. Richardson, Inefficient muscular stabilization of the lumbar spine associated with low back pain. A motor control evaluation of transversus abdominis, *Spine (Phila Pa 1976)* 21 (1996) 2640–2650, doi:[10.1097/00007632-199611150-00014](https://doi.org/10.1097/00007632-199611150-00014).
- [8] J.H. van Dieen, J. Cholewicki, A. Radebold, Trunk muscle recruitment patterns in patients with low back pain enhance the stability of the lumbar spine, *Spine (Phila Pa 1976)* 28 (2003) 834–841, doi:[10.1097/01.BRS.0000058939.51147.55](https://doi.org/10.1097/01.BRS.0000058939.51147.55).
- [9] L.E. Miller, J.E. Urban, M.E. Kelley, A.K. Powers, C.T. Whitlow, J.A. Maldjian, S. Rowson, J.D. Stitzel, Evaluation of Brain Response during Head Impact in Youth Athletes Using an Anatomically Accurate Finite Element Model, *J. Neurotrauma* 36 (2019) 1561–1570, doi:[10.1089/neu.2018.6037](https://doi.org/10.1089/neu.2018.6037).
- [10] J. Row, L. Chan, D. Damiano, C. Shenouda, J. Collins, C. Zampieri, Balance Assessment in Traumatic Brain Injury: a Comparison of the Sensory Organization and Limits of Stability Tests, *J. Neurotrauma* 36 (2019) 2435–2442, doi:[10.1089/neu.2018.5755](https://doi.org/10.1089/neu.2018.5755).
- [11] E.A. Keshner, Vestibulocollic and Cervicocollic Control, in: M.D. Binder, N. Hirokawa, U. Windhorst (Eds.), *Encyclopedia of Neuroscience*, Springer Berlin Heidelberg, Berlin, Heidelberg, 2009, pp. 4220–4224.
- [12] R.J. Peterka, M.S. Benolken, Role of somatosensory and vestibular cues in attenuating visually induced human postural sway, *Exp. Brain Res.* 105 (1995) 101–110, doi:[10.1007/BF00242186](https://doi.org/10.1007/BF00242186).
- [13] K.E. Cullen, O.A. Zobeiri, Proprioception and the predictive sensing of active self-motion, *Current Opinion in Physiology* 20 (2021) 29–38, doi:[10.1016/j.cophys.2020.12.001](https://doi.org/10.1016/j.cophys.2020.12.001).
- [14] V.E. Pettorossi, M. Schieppati, Neck proprioception shapes body orientation and perception of motion, *Front Hum Neurosci* 8 (2014) 895, doi:[10.3389/fnhum.2014.00895](https://doi.org/10.3389/fnhum.2014.00895).
- [15] U. Proske, S.C. Gandevia, Kinesthetic Senses, *Compr Physiol* 8 (2018) 1157–1183, doi:[10.1002/cphy.c170036](https://doi.org/10.1002/cphy.c170036).
- [16] R.A. Grünewald, Y. Yoneda, J.M. Shipman, H.J. Sagar, Idiopathic focal dystonia: a disorder of muscle spindle afferent processing? *Brain* 120 (Pt 12) (1997) 2179–2185, doi:[10.1093/brain/120.12.2179](https://doi.org/10.1093/brain/120.12.2179).
- [17] K.H. Yang, F. Zhu, F. Luan, L. Zhao, P.C. Begeman, Development of a finite element model of the human neck, *SAE Tech Pap* (1998).
- [18] Y.-C. Deng, X. Li, Y. Liu, Modeling of the human cervical spine using finite element techniques, *SAE Tech Pap* (1999).
- [19] K. Brolin, P. Halldin, Development of a finite element model of the upper cervical spine and a parameter study of ligament characteristics, *Spine (Phila Pa 1976)* 29 (2004) 376–385, doi:[10.1097/01.brs.000009082.99182.2d](https://doi.org/10.1097/01.brs.000009082.99182.2d).
- [20] Y. Kitagawa, T. Yasuki, J. Hasegawa, Research study on neck injury lessening with active head restraint using human body FE model, *Traffic Inj. Prev.* 9 (2008) 574–582, doi:[10.1080/15389580802381954](https://doi.org/10.1080/15389580802381954).
- [21] M.L. Davis, B. Koya, J.M. Schap, F.S. Gayzik, Development and Full Body Validation of a 5th Percentile Female Finite Element Model, *Stapp Car Crash J* 60 (2016) 509–544, doi:[10.4271/2016-22-0015](https://doi.org/10.4271/2016-22-0015).
- [22] D. Schwartz, B. Guleyupoglu, B. Koya, J.D. Stitzel, F.S. Gayzik, Development of a computationally efficient full human body finite element model, *Traffic Inj. Prev.* 16 (Suppl 1) (2015) S49–S56, doi:[10.1080/15389588.2015.1021418](https://doi.org/10.1080/15389588.2015.1021418).
- [23] J. Osth, K. Brolin, M.Y. Svensson, A. Linder, A Female Ligamentous Cervical Spine Finite Element Model Validated for Physiological Loads, *J. Biomech. Eng.* 138 (2016) 061005, doi:[10.1115/1.4032966](https://doi.org/10.1115/1.4032966).
- [24] J.B. Fice, D.S. Cronin, M.B. Panzer, Cervical spine model to predict capsular ligament response in rear impact, *Ann. Biomed. Eng.* 39 (2011) 2152–2162, doi:[10.1007/s10439-011-0315-4](https://doi.org/10.1007/s10439-011-0315-4).
- [25] M.B. Panzer, J.B. Fice, D.S. Cronin, Cervical spine response in frontal crash, *Med. Eng. Phys.* 33 (2011) 1147–1159, doi:[10.1016/j.medengphy.2011.05.004](https://doi.org/10.1016/j.medengphy.2011.05.004).
- [26] I.P.A. Putra, J. Iraeus, R. Thomson, M.Y. Svensson, A. Linder, F. Sato, Comparison of control strategies for the cervical muscles of an average female head-neck finite element model, *Traffic Inj. Prev.* 20 (2019) S116–S122, doi:[10.1080/15389588.2019.1670818](https://doi.org/10.1080/15389588.2019.1670818).
- [27] I.P.A. Putra, J. Iraeus, F. Sato, M.Y. Svensson, A. Linder, R. Thomson, Optimization of Female Head-Neck Model with Active Reflexive Cervical Muscles in Low Severity Rear Impact Collisions, *Ann. Biomed. Eng.* 49 (2021) 115–128, doi:[10.1007/s10439-020-02512-1](https://doi.org/10.1007/s10439-020-02512-1).
- [28] D. Salin, P.-J. Arnoux, K. Kayvantash, M. Behr, Implementation of reflex loops in a biomechanical finite element model, *Comput Methods Biomed Engin* 19 (2016) 1578–1582, doi:[10.1080/10255842.2016.1170123](https://doi.org/10.1080/10255842.2016.1170123).
- [29] F. Mo, F. Li, M. Behr, Z. Xiao, G. Zhang, X. Du, A Lower Limb-Pelvis Finite Element Model with 3D Active Muscles, *Ann Biomed Eng* 46 (2018) 86–96, doi:[10.1007/s10439-017-1942-1](https://doi.org/10.1007/s10439-017-1942-1).
- [30] F. Mo, J. Li, M. Dan, T. Liu, M. Behr, Implementation of controlling strategy in a biomechanical lower limb model with active muscles for coupling multibody dynamics and finite element analysis, *J. Biomech.* 91 (2019) 51–60, doi:[10.1016/j.jbiomech.2019.05.001](https://doi.org/10.1016/j.jbiomech.2019.05.001).
- [31] R. Happee, E. de Bruijn, P.A. Forbes, F.C.T. van der Helm, Dynamic head-neck stabilization and modulation with perturbation bandwidth investigated using a multisegment neuromuscular model, *J. Biomech.* 58 (2017) 203–211, doi:[10.1016/j.jbiomech.2017.05.005](https://doi.org/10.1016/j.jbiomech.2017.05.005).
- [32] H. Zhang, F. Mo, L. Wang, M. Behr, P.J. Arnoux, A Framework of a Lower Limb Musculoskeletal Model With Implemented Natural Proprioceptive Feedback and Its Progressive Evaluation, *IEEE Trans. Neural Syst. Rehabil. Eng.* 28 (2020) 1866–1875, doi:[10.1109/TNSRE.2020.3003497](https://doi.org/10.1109/TNSRE.2020.3003497).
- [33] F. Mo, Q. Zhang, H. Zhang, J. Long, Y. Wang, G. Chen, J. Ye, A simulation-based framework with a proprioceptive musculoskeletal model for evaluating the rehabilitation oskeleton system, *Comput. Methods Programs Biomed.* 208 (2021) 106270, doi:[10.1016/j.cmpb.2021.106270](https://doi.org/10.1016/j.cmpb.2021.106270).
- [34] Z. Zheng, F. Mo, T. Liu, X. Li, A novel neuromuscular head-neck model and its application on impact analysis, *IEEE Trans. Neural Syst. Rehabil. Eng.* (2021), doi:[10.1109/tnsre.2021.3095624](https://doi.org/10.1109/tnsre.2021.3095624).
- [35] M.M. Panjabi, J. Cholewicki, K. Nibu, J.N. Grauer, L.B. Babat, J. Dvorak, Mechanism of whiplash injury, *Clin. Biomech. (Bristol, Avon)* 13 (1998) 239–249, doi:[10.1016/s0268-0033\(98\)00033-3](https://doi.org/10.1016/s0268-0033(98)00033-3).
- [36] K. Pastakia, S. Kumar, Acute whiplash associated disorders (WAD), *Open Access Emerg Med* 3 (2011) 29–32, doi:[10.2147/oam.S17853](https://doi.org/10.2147/oam.S17853).
- [37] W.O. Spitzer, M.L. Skovron, L.R. Salmi, J.D. Cassidy, J. Duranteau, S. Suissa, E. Zeiss, Scientific monograph of the Quebec Task Force on Whiplash-Associated Disorders: redefining "whiplash" and its management, *Spine (Phila Pa 1976)* 20 (1995) 1s–73s.
- [38] M. Yu, W.K. Zhao, M. Li, S.B. Wang, Y. Sun, L. Jiang, F. Wei, X.G. Liu, L. Zeng, Z.J. Liu, Analysis of cervical and global spine alignment under Roussouly sagittal classification in Chinese cervical spondylotic patients and asymptomatic subjects, *Eur. Spine J.* 24 (2015) 1265–1273, doi:[10.1007/s00586-015-3832-2](https://doi.org/10.1007/s00586-015-3832-2).
- [39] W. Zhu, S. Sha, Z. Liu, Y. Li, L. Xu, W. Zhang, Y. Qiu, Z. Zhu, Influence of the Occipital Orientation on Cervical Sagittal Alignment: a Prospective Radiographic Study on 335 Normal Subjects, *Sci. Rep.* 8 (2018) 15336, doi:[10.1038/s41598-018-33287-0](https://doi.org/10.1038/s41598-018-33287-0).
- [40] M.M. Panjabi, N.C. Chen, E.K. Shin, J.L. Wang, The cortical shell architecture of human cervical vertebral bodies, *Spine (Phila Pa 1976)* 26 (2001) 2478–2484, doi:[10.1097/00007632-200111150-00016](https://doi.org/10.1097/00007632-200111150-00016).
- [41] H. Gray, *Anatomy of the Human Body*, Lea & Febiger, 1878.
- [42] F.H. Netter, *Atlas of human anatomy*, Professional Edition E-Book: including NetterReference.com Access with full downloadable image Bank, Elsevier health sci (2014).
- [43] M.B. Panzer, D.S. Cronin, C4-C5 segment finite element model development, validation, and load-sharing investigation, *J. Biomech.* 42 (2009) 480–490, doi:[10.1016/j.jbiomech.2008.11.036](https://doi.org/10.1016/j.jbiomech.2008.11.036).
- [44] T.-W.D. Shen, Investigation of Whiplash Associated Disorders using Finite Element Neck Models With Active Musculature in Frontal, Rear and Lateral Impact, Univ Waterloo, 2020.
- [45] J. Dvorak, E. Schneider, P. Saldinger, B. Rahn, Biomechanics of the craniocervical region: the alar and transverse ligaments, *J. Orthop. Res.* 6 (1988) 452–461, doi:[10.1002/jor.1100060317](https://doi.org/10.1002/jor.1100060317).
- [46] N. Bailly, L. Diotalevi, M.H. Beausejour, E. Wagnac, J.M. Mac-Thiong, Y. Petit, Numerical investigation of the relative effect of disc bulging and ligamentum flavum hypertrophy on the mechanism of central cord syndrome, *Clin. Biomech. (Bristol, Avon)* 74 (2020) 58–65, doi:[10.1016/j.clinbiomech.2020.02.008](https://doi.org/10.1016/j.clinbiomech.2020.02.008).
- [47] L. Fradet, P.-J. Arnoux, V. Callot, Y. Petit, Geometrical variations in white and gray matter affect the biomechanics of spinal cord injuries more than the arachnoid space, *Adv Mech Eng* 8 (2016), doi:[10.1177/1687814016664703](https://doi.org/10.1177/1687814016664703).
- [48] L. Diotalevi, N. Bailly, E. Wagnac, J.M. Mac-Thiong, J. Goulet, Y. Petit, Dynamics of spinal cord compression with different patterns of thoracolumbar burst fractures: numerical simulations using finite element modelling, *Clin. Biomech. (Bristol, Avon)* 72 (2020) 186–194, doi:[10.1016/j.clinbiomech.2019.12.023](https://doi.org/10.1016/j.clinbiomech.2019.12.023).
- [49] M. Dreischarf, T. Zander, A. Shirazi-Adl, C.M. Puttlitz, C.J. Adam, C.S. Chen, V.K. Goel, A. Kiapour, Y.H. Kim, K.M. Labus, J.P. Little, W.M. Park, Y.H. Wang, H.J. Wilke, A. Rohlmann, H. Schmidt, Comparison of eight published static finite element models of the intact lumbar spine: predictive power of models improves when combined together, *J. Biomech.* 47 (2014) 1757–1766, doi:[10.1016/j.jbiomech.2014.04.002](https://doi.org/10.1016/j.jbiomech.2014.04.002).
- [50] S. Jannesar, B. Nadler, C.J. Sparrey, The Transverse Isotropy of Spinal Cord White Matter Under Dynamic Load, *J. Biomech. Eng.* 138 (2016), doi:[10.1115/1.4034171](https://doi.org/10.1115/1.4034171).
- [51] M. Fournely, Y. Petit, E. Wagnac, M. Evin, P.J. Arnoux, Effect of experimental, morphological and mechanical factors on the murine spinal cord subjected to transverse contusion: a finite element study, *PLOS ONE* 15 (2020) e0232975, doi:[10.1371/journal.pone.0232975](https://doi.org/10.1371/journal.pone.0232975).

- [52] S. Jannesar, M. Allen, S. Mills, A. Gibbons, J.C. Bresnahan, E.A. Salegio, C.J. Sparrey, Compressive mechanical characterization of non-human primate spinal cord white matter, *Acta Biomater.* 74 (2018) 260–269, doi:[10.1016/j.actbio.2018.05.002](https://doi.org/10.1016/j.actbio.2018.05.002).
- [53] J.D. John, N. Yoganandan, M.W.J. Arun, G. Saravana Kumar, Influence of morphological variations on cervical spine segmental responses from inertial loading, *Traffic Inj. Prev.* 19 (2018) S29–S36, doi:[10.1080/15389588.2017.1403017](https://doi.org/10.1080/15389588.2017.1403017).
- [54] J. Borst, P.A. Forbes, R. Happee, D.H. Veeger, Muscle parameters for musculoskeletal modelling of the human neck, *Clin. Biomech. (Bristol, Avon)* 26 (2011) 343–351, doi:[10.1016/j.clinbiomech.2010.11.019](https://doi.org/10.1016/j.clinbiomech.2010.11.019).
- [55] L.K. Kamibayashi, F.J. Richmond, Morphometry of human neck muscles, *Spine (Phila Pa 1976)* 23 (1998) 1314–1323, doi:[10.1097/00007632-199806150-00005](https://doi.org/10.1097/00007632-199806150-00005).
- [56] C. Van Ee, A. Chasse, B. Myers, Quantifying skeletal muscle properties in cadaveric test specimens: effects of mechanical loading, postmortem time, and freezer storage, *J. Biomech. Eng.* 122 (2000) 9–14, doi:[10.1115/1.429621](https://doi.org/10.1115/1.429621).
- [57] L. Tsou, *The Effects of Muscle Aging On Hyoid Motion During swallowing: a Study Using a 3D Biomechanical Model*, Univ British Columbia, 2012.
- [58] J. Östh, K. Brolin, S. Carlsson, J. Wismans, J. Davidsson, The occupant response to autonomous braking: a modeling approach that accounts for active musculature, *Traffic Inj. Prev.* 13 (2012) 265–277, doi:[10.1080/15389588.2011.649437](https://doi.org/10.1080/15389588.2011.649437).
- [59] J. Osth, M. Mendoza-Vazquez, F. Sato, M.Y. Svensson, A. Linder, K. Brolin, A female head-neck model for rear impact simulations, *J. Biomech.* 51 (2017) 49–56, doi:[10.1016/j.jbiomech.2016.11.066](https://doi.org/10.1016/j.jbiomech.2016.11.066).
- [60] J.D. Mortensen, A.N. Vasavada, A.S. Merryweather, The inclusion of hyoid muscles improve moment generating capacity and dynamic simulations in musculoskeletal models of the head and neck, *PLoS ONE* 13 (2018) e0199912, doi:[10.1371/journal.pone.0199912](https://doi.org/10.1371/journal.pone.0199912).
- [61] J.M. Winters, L. Stark, Estimated mechanical properties of synergistic muscles involved in movements of a variety of human joints, *J. Biomech.* 21 (1988) 1027–1041, doi:[10.1016/0021-9290\(88\)90249-7](https://doi.org/10.1016/0021-9290(88)90249-7).
- [62] J.M. Winters, L. Stark, Analysis of fundamental human movement patterns through the use of in-depth antagonistic muscle models, *IEEE Trans. Biomed. Eng.* 32 (1985) 826–839, doi:[10.1109/tbme.1985.325498](https://doi.org/10.1109/tbme.1985.325498).
- [63] A.N. Vasavada, J. Danaraj, G.P. Siegmund, Head and neck anthropometry, vertebral geometry and neck strength in height-matched men and women, *J. Biomech.* 41 (2008) 114–121, doi:[10.1016/j.jbiomech.2007.07.007](https://doi.org/10.1016/j.jbiomech.2007.07.007).
- [64] M. Fournely, Y. Petit, É. Wagnac, J. Laurin, V. Callot, P.J. Arnoux, High-speed video analysis improves the accuracy of spinal cord compression measurement in a mouse contusion model, *J. Neurosci. Methods* 293 (2018) 1–5, doi:[10.1016/j.jneumeth.2017.09.007](https://doi.org/10.1016/j.jneumeth.2017.09.007).
- [65] J.B. Myklebust, F. Pintar, N. Yoganandan, J.F. Cusick, D. Maiman, T.J. Myers, A. Sances Jr., Tensile strength of spinal ligaments, *Spine (Phila Pa 1976)* 13 (1988) 526–531.
- [66] S.F. Mattucci, J.A. Moulton, N. Chandrashekhar, D.S. Cronin, Strain rate dependent properties of human craniocervical ligaments, *J. Mech. Behav. Biomed. Mater.* 23 (2013) 71–79, doi:[10.1016/j.jmbbm.2013.04.005](https://doi.org/10.1016/j.jmbbm.2013.04.005).
- [67] S.F. Mattucci, D.S. Cronin, A method to characterize average cervical spine ligament response based on raw data sets for implementation into injury biomechanics models, *J. Mech. Behav. Biomed. Mater.* 41 (2015) 251–260, doi:[10.1016/j.jmbbm.2014.09.023](https://doi.org/10.1016/j.jmbbm.2014.09.023).
- [68] M. Shea, W.T. Edwards, A.A. White, W.C. Hayes, Variations of stiffness and strength along the human cervical spine, *J. Biomech.* 24 (1991) 95–107, doi:[10.1016/0021-9290\(91\)90354-p](https://doi.org/10.1016/0021-9290(91)90354-p).
- [69] R.W. Nightingale, B.A. Winkelstein, K.E. Knaub, W.J. Richardson, J.F. Luck, B.S. Myers, Comparative strengths and structural properties of the upper and lower cervical spine in flexion and extension, *J. Biomech.* 35 (2002) 725–732, doi:[10.1016/s0021-9290\(02\)00037-4](https://doi.org/10.1016/s0021-9290(02)00037-4).
- [70] R.W. Nightingale, V. Carol Chancey, D. Ottaviano, J.F. Luck, L. Tran, M. Prange, B.S. Myers, Flexion and extension structural properties and strengths for male cervical spine segments, *J. Biomech.* 40 (2007) 535–542, doi:[10.1016/j.jbiomech.2006.02.015](https://doi.org/10.1016/j.jbiomech.2006.02.015).
- [71] J.A. Wheeldon, F.A. Pintar, S. Knowles, N. Yoganandan, Experimental flexion/extension data corridors for validation of finite element models of the young, normal cervical spine, *J. Biomech.* 39 (2006) 375–380, doi:[10.1016/j.jbiomech.2004.11.014](https://doi.org/10.1016/j.jbiomech.2004.11.014).
- [72] M.M. Panjabi, J.J. Crisco, A. Vasavada, T. Oda, J. Cholewicki, K. Nibu, E. Shin, Mechanical properties of the human cervical spine as shown by three-dimensional load-displacement curves, *Spine (Phila Pa 1976)* 26 (2001) 2692–2700, doi:[10.1097/00007632-200112150-00012](https://doi.org/10.1097/00007632-200112150-00012).
- [73] N.A. White, P.C. Begeman, W.N. Hardy, K.H. Yang, K. Ono, F. Sato, K. Kamiji, T. Yasuki, M.J. Bey, Investigation of upper body and cervical spine kinematics of post mortem human subjects (PMHS) during low-speed, rear-end impacts, *SAE Tech Pap* (2009).
- [74] F. Mo, D. Luo, Z. Tan, B. Shang, X. Lv, D. Zhou, A Human Active Lower Limb Model for Chinese Pedestrian Safety Evaluation, *J. Bionic Eng.* 18 (2021) 1–15, doi:[10.1007/s42235-021-0067-2](https://doi.org/10.1007/s42235-021-0067-2).
- [75] K. Ono, S. Inami, K. Kaneoka, T. Gotou, Y. Kisanuki, S. Sakuma, K. Miki, Relationship between localized spine deformation and cervical vertebral motions for low speed rear impacts using human volunteers, *SAE Tech Pap* (1999).
- [76] F. Mo, J. Li, M. Dan, T. Liu, M. Behr, Implementation of controlling strategy in a biomechanical lower limb model with active muscles for coupling multibody dynamics and finite element analysis, *J. Biomech.* 91 (2019) 51–60, doi:[10.1016/j.jbiomech.2019.05.001](https://doi.org/10.1016/j.jbiomech.2019.05.001).
- [77] M.J. Devivo, Epidemiology of traumatic spinal cord injury: trends and future implications, *Spinal Cord* 50 (2012) 365–372, doi:[10.1038/sc.2011.178](https://doi.org/10.1038/sc.2011.178).
- [78] D.L. Kreipke, K.R. Gillespie, M.C. McCarthy, J.T. Mail, J.C. Lappas, T.A. Broadie, Reliability of indications for cervical spine films in trauma patients, *J. Trauma* 29 (1989) 1438–1439, doi:[10.1097/00005373-198910000-00024](https://doi.org/10.1097/00005373-198910000-00024).
- [79] S.J. Rizzolo, M.R. Piazza, J.M. Cotler, R.A. Balderston, D. Schaefer, A. Flanders, Intervertebral disc injury complicating cervical spine trauma, *Spine (Phila Pa 1976)* 16 (1991) S187–S189, doi:[10.1097/00007632-199106001-00002](https://doi.org/10.1097/00007632-199106001-00002).
- [80] D.C. Burke, H.T. Burley, G.H. Ungar, Data on spinal injuries—Part I. Collection and analysis of 352 consecutive admissions, *Aust. N. Z. J. Surg.* 55 (1985) 3–12, doi:[10.1111/j.1445-2197.1985.tb00846.x](https://doi.org/10.1111/j.1445-2197.1985.tb00846.x).
- [81] N. Yoganandan, M. Haffner, D.J. Maiman, H. Nichols, F.A. Pintar, J. Jentzen, S.S. Weinshel, S.J. Larson, A. Sances, Epidemiology and Injury Biomechanics of Motor Vehicle Related Trauma to the Human Spine, *SAE Transactions* 98 (1989) 1790–1809, doi:[10.4271/892438](https://doi.org/10.4271/892438).
- [82] V.S. Prasad, A. Schwartz, R. Bhutani, P.W. Sharkey, M.L. Schwartz, Characteristics of injuries to the cervical spine and spinal cord in polytrauma patient population: experience from a regional trauma unit, *Spinal Cord* 37 (1999) 560–568, doi:[10.1038/sj.sc.3100878](https://doi.org/10.1038/sj.sc.3100878).
- [83] I. Koyanagi, Y. Iwasaki, K. Hida, M. Akino, H. Imamura, H. Abe, Acute cervical cord injury without fracture or dislocation of the spinal column, *J. Neurosurg.* 93 (2000) 15–20, doi:[10.3171/spi.2000.93.1.0015](https://doi.org/10.3171/spi.2000.93.1.0015).
- [84] P. O'Connor, Incidence and patterns of spinal cord injury in Australia, *Accid. Anal. Prev.* 34 (2002) 405–415, doi:[10.1016/s0001-4575\(01\)00036-7](https://doi.org/10.1016/s0001-4575(01)00036-7).
- [85] R.J. O'Connor, P.C. Murray, Review of spinal cord injuries in Ireland, *Spinal Cord* 44 (2006) 445–448, doi:[10.1038/sj.sc.3101856](https://doi.org/10.1038/sj.sc.3101856).
- [86] C. Ye, T. Sun, J. Li, F. Zhang, Pattern of sports- and recreation-related spinal cord injuries in Beijing, *Spinal Cord* 47 (2009) 857–860, doi:[10.1038/sc.2009.49](https://doi.org/10.1038/sc.2009.49).
- [87] G.Z. Ning, T.Q. Yu, S.Q. Feng, X.H. Zhou, D.X. Ban, Y. Liu, X.X. Jiao, Epidemiology of traumatic spinal cord injury in Tianjin, China, *Spinal Cord* 49 (2011) 386–390, doi:[10.1038/sc.2010.130](https://doi.org/10.1038/sc.2010.130).
- [88] Q. Wu, Y.L. Li, G.Z. Ning, S.Q. Feng, T.C. Chu, Y. Li, Y. Hao, Q.L. Wu, Epidemiology of traumatic cervical spinal cord injury in Tianjin, China, *Spinal Cord* 50 (2012) 740–744, doi:[10.1038/sc.2012.42](https://doi.org/10.1038/sc.2012.42).
- [89] Y. Zhou, X.B. Wang, S.L. Kan, G.Z. Ning, Y.L. Li, B. Yang, Y. Li, J.C. Sun, S.Q. Feng, Traumatic spinal cord injury in Tianjin, China: a single-center report of 354 cases, *Spinal Cord* 54 (2016) 670–674, doi:[10.1038/sc.2015.173](https://doi.org/10.1038/sc.2015.173).
- [90] G.Z. Ning, Z.P. Mu, L. Shangguan, Y. Tang, C.Q. Li, Z.F. Zhang, Y. Zhou, Epidemiological features of traumatic spinal cord injury in Chongqing, China, *J. Spinal Cord. Med.* 39 (2016) 455–460, doi:[10.1080/10790268.2015.1101982](https://doi.org/10.1080/10790268.2015.1101982).
- [91] N.S.C.I.S. Center, *Annual Statistical Report for the Spinal Cord Injury Model Systems Public version, Complete Public Version*, University of Alabama at Birmingham, Back to cited text, Birmingham, Alabama, 2017.
- [92] D. Krappinger, R.A. Lindtner, M.J. Zegg, B. Henninger, V. Kaser, A. Spicher, R. Schmid, Spondylolytic traumatic central cord syndrome: a hidden dislodgement injury? *European Spine Journal* 28 (2019) 434–441, doi:[10.1007/s00586-018-5796-5](https://doi.org/10.1007/s00586-018-5796-5).
- [93] A. Montoto-Marques, M.E. Ferreiro-Velasco, S. Salvador-de la Barrera, V. Balboa-Barreiro, A. Rodriguez-Sotillo, R. Mejijide-Failde, Epidemiology of traumatic spinal cord injury in Galicia, Spain: trends over a 20-year period, *Spinal Cord* 55 (2017) 588–594, doi:[10.1038/sc.2017.13](https://doi.org/10.1038/sc.2017.13).
- [94] Y. Liu, J.X. Xie, F. Niu, Z. Xu, P. Tan, C. Shen, H. Gao, S. Liu, Z. Ma, K.F. So, W. Wu, C. Chen, S. Gao, X.M. Xu, H. Zhu, Surgical intervention combined with weight-bearing walking training improves neurological recoveries in 320 patients with clinically complete spinal cord injury: a prospective self-controlled study, *Neural Regen Res* 16 (2021) 820–829, doi:[10.4103/1673-5374.297080](https://doi.org/10.4103/1673-5374.297080).
- [95] J. Šrámek, J. Stulík, P. Sebesta, T. Vyskocil, J. Kryl, P. Nesnídal, M. Barna, Hyperextension trauma in patients with cervical spondylosis, *Acta Chir. Orthop. Traumatol. Cech.* 76 (2009) 128–132.
- [96] T. Maeda, T. Ueta, E. Mori, I. Yugue, O. Kawano, T. Takao, H. Sakai, S. Okada, K. Shiba, Soft-Tissue Damage and Segmental Instability in Adult Patients With Cervical Spinal Cord Injury Without Major Bone Injury, *Spine* 37 (2012) E1560–E1566, doi:[10.1097/BRS.0b013e318272f345](https://doi.org/10.1097/BRS.0b013e318272f345).
- [97] M.M. Panjabi, S. Ito, P.C. Ivancic, W. Rubin, Evaluation of the intervertebral neck injury criterion using simulated rear impacts, *J. Biomech.* 38 (2005) 1694–1701, doi:[10.1016/j.jbiomech.2004.07.015](https://doi.org/10.1016/j.jbiomech.2004.07.015).
- [98] V. Janda, The Cervico-Cervical Junction. A Neglected Clinical Entity, *J Orthop Med* 24 (2002) 77–78, doi:[10.1080/1355297X.2002.11736169](https://doi.org/10.1080/1355297X.2002.11736169).
- [99] N.E. Epstein, R. Hollingsworth, Diagnosis and management of traumatic cervical central spinal cord injury: a review, *Surg Neurol Int* 6 (2015) S140–S153, doi:[10.4103/2152-7806.156552](https://doi.org/10.4103/2152-7806.156552).
- [100] M. Sturzenegger, G. DiStefano, B.P. Radanov, A. Schnidrig, Presenting symptoms and signs after whiplash injury: the influence of accident mechanisms, *Neurology* 44 (1994) 688–693, doi:[10.1212/wnl.44.4.688](https://doi.org/10.1212/wnl.44.4.688).
- [101] E.J.M. Hendriks, G.G.M. Scholten-Peeters, D. van der Windt, C.W.M. Neeleman-van der Steen, R.A.B. Oostendorp, A.P. Verhagen, Prognostic factors for poor recovery in acute whiplash patients, *Pain* 114 (2005) 408–416, doi:[10.1016/j.pain.2005.01.006](https://doi.org/10.1016/j.pain.2005.01.006).
- [102] W.J. Anderst, W.F. Donaldson 3rd, J.Y. Lee, J.D. Kang, Cervical motion segment percent contributions to flexion-extension during continuous functional movement in control subjects and arthrodesis patients, *Spine (Phila Pa 1976)* 38 (2013) E533–E539, doi:[10.1097/BRS.0b013e318289378a](https://doi.org/10.1097/BRS.0b013e318289378a).
- [103] R.W. Evans, Some observations on whiplash injuries, *Neurol. Clin.* 10 (1992) 975–997, doi:[10.1016/s0733-8619\(18\)30191-9](https://doi.org/10.1016/s0733-8619(18)30191-9).

- [104] S.J. Davis, L.M. Teresi, W.G. Bradley Jr., M.A. Ziembka, A.E. Bloze, Cervical spine hyperextension injuries: MR findings, *Radiology* 180 (1991) 245–251, doi:[10.1148/radiology.180.1.2052703](https://doi.org/10.1148/radiology.180.1.2052703).
- [105] J. Gershon-Cohen, E. Budin, F. Glauser, WHIPLASH FRACTURES OF CERVICODORSAL SPINOUS PROCESSES: RESEMBLANCE TO SHOVELER'S FRACTURE, *JAMA* 155 (1954) 560–561, doi:[10.1001/jama.1954.03690240026007](https://doi.org/10.1001/jama.1954.03690240026007).
- [106] A. Stäbler, J. Eck, R. Penning, S.P. Milz, R. Bartl, D. Resnick, M. Reiser, Cervical spine: postmortem assessment of accident injuries—comparison of radiographic, MR imaging, anatomic, and pathologic findings, *Radiology* 221 (2001) 340–346, doi:[10.1148/radiol.2212010336](https://doi.org/10.1148/radiol.2212010336).
- [107] H.J. Griffiths, A.S. Kidwai, W.C. Wright, Hyperextension Strain or Whiplash Injuries to the Cervical Spine—Revisited, *Journal of Whiplash & Related Disorders* 3 (2004) 25–45, doi:[10.3109/J180v03n01_04](https://doi.org/10.3109/J180v03n01_04).
- [108] H. Jónsson Jr., K. Cesarin, B. Sahlstedt, W. Rauschning, Findings and outcome in whiplash-type neck distortions, *Spine (Phila Pa 1976)* 19 (1994) 2733–2743, doi:[10.1097/000007632-199412150-00001](https://doi.org/10.1097/000007632-199412150-00001).
- [109] A.J. Hamer, M.F. Gargan, G.C. Bannister, R.J. Nelson, Whiplash injury and surgically treated cervical disc disease, *Injury* 24 (1993) 549–550, doi:[10.1016/0020-1383\(93\)90035-5](https://doi.org/10.1016/0020-1383(93)90035-5).
- [110] K. Pettersson, C. Hildingsson, G. Toolanen, M. Fagerlund, J. Björnebrink, MRI and neurology in acute whiplash trauma. No correlation in prospective examination of 39 cases, *Acta Orthop. Scand.* 65 (1994) 525–528, doi:[10.3109/17453679409000906](https://doi.org/10.3109/17453679409000906).
- [111] A. Kongsted, J.S. Sorensen, H. Andersen, B. Keseler, T.S. Jensen, T. Bendix, Are early MRI findings correlated with long-lasting symptoms following whiplash injury? A prospective trial with 1-year follow-up, *Eur. Spine J.* 17 (2008) 996–1005, doi:[10.1007/s00586-008-0687-9](https://doi.org/10.1007/s00586-008-0687-9).
- [112] N. Bogduk, On cervical zygapophysial joint pain after whiplash, *Spine (Phila Pa 1976)* 36 (2011) S194–S199, doi:[10.1097/BRS.0b013e3182387f1d](https://doi.org/10.1097/BRS.0b013e3182387f1d).
- [113] F. Li, N.-s. Liu, H.-g. Li, B. Zhang, S.-w. Tian, M.-g. Tan, B. Sandoz, A review of neck injury and protection in vehicle accidents, *Transp Saf Environ* 1 (2019) 89–105, doi:[10.1093/tse/tdz012](https://doi.org/10.1093/tse/tdz012).
- [114] S. Park, S. Lee, J. Yoon, S.W. Chae, Finite element analysis of knee and ankle joint during gait based on motion analysis, *Med. Eng. Phys.* 63 (2019) 33–41, doi:[10.1016/j.medengphy.2018.11.003](https://doi.org/10.1016/j.medengphy.2018.11.003).
- [115] M.A. Correia, S.D. McLachlin, D.S. Cronin, Vestibulocollic and Cervicocollic Muscle Reflexes in a Finite Element Neck Model During Multidirectional Impacts, *Ann. Biomed. Eng.* 49 (2021) 1645–1656, doi:[10.1007/s10439-021-02783-2](https://doi.org/10.1007/s10439-021-02783-2).
- [116] T. Gotou, K. Ono, M. Ito, F. Matuoka, A comparison between BioRID AND Hybrid III head/neck/torso response in middle speed sled rear impact tests, *SAE Tech Pap* (2001).
- [117] J. Davidsson, P. Lövsund, K. Ono, M.Y. Svensson, S. Inami, A comparison of volunteer, BioRID P3 and Hybrid III performance in rear impacts, *Traffic Inj. Prev.* (2) (2001) 203–220, doi:[10.1080/10286580108902565](https://doi.org/10.1080/10286580108902565).
- [118] M. Kleinberger, L. Voo, A. Merkle, R. Szczepanowski, B. McGee, A comparative study of dummy sensitivity to seat design parameters, in: Proceedings of the 20th International Technical Conference on Enhanced safety of vehicles, Lyon, France, 2007, pp. 18–21.
- [119] B. Aldman, An Analytical Approach to the Impact Biomechanics of Head and Neck Injury, *Proceedings: American Association for Automotive Medicine Annual Conference* 30 (1986) 439–454.
- [120] M.Y. Svensson, Neck-Injuries in Rear-End Car Collisions: Sites and Biomechanical Causes of the Injuries, Test Methods and Preventive Measures, Doctor Thesis Crash safety Division, Chalmers University of Technology, Gothenburg, Sweden, 1993.
- [121] E. Rydman, P. Kasina, S. Ponzer, H. Jarnbert-Pettersson, Association between cervical degeneration and self-perceived nonrecovery after whiplash injury, *Spine J.* 19 (2019) 1986–1994, doi:[10.1016/j.spinee.2019.07.017](https://doi.org/10.1016/j.spinee.2019.07.017).
- [122] B.R. Kaale, J. Krakenes, G. Albrektsen, K. Wester, Head position and impact direction in whiplash injuries: associations with MRI-verified lesions of ligaments and membranes in the upper cervical spine, *J. Neurotrauma* 22 (2005) 1294–1302, doi:[10.1089/neu.2005.22.1294](https://doi.org/10.1089/neu.2005.22.1294).
- [123] M.H. Beausejour, Y. Petit, J. Hagen, P.J. Arnoux, J.M. Thiong, E. Wagnac, Contribution of injured posterior ligamentous complex and intervertebral disc on post-traumatic instability at the cervical spine, *Comput Methods Biomed Engin* (2020) 1–12, doi:[10.1080/10255842.2020.1767776](https://doi.org/10.1080/10255842.2020.1767776).
- [124] B.R. Kaale, J. Krakenes, G. Albrektsen, K. Wester, Whiplash-associated disorders impairment rating: neck disability index score according to severity of MRI findings of ligaments and membranes in the upper cervical spine, *J. Neurotrauma* 22 (2005) 466–475, doi:[10.1089/neu.2005.22.466](https://doi.org/10.1089/neu.2005.22.466).
- [125] C.Y. Greaves, M.S. Gadala, T.R. Oxland, A three-dimensional finite element model of the cervical spine with spinal cord: an investigation of three injury mechanisms, *Ann. Biomed. Eng.* 36 (2008) 396–405, doi:[10.1007/s10439-008-9440-0](https://doi.org/10.1007/s10439-008-9440-0).
- [126] G.P. Siegmund, B.A. Winkelstein, P.C. Ivancic, M.Y. Svensson, A. Vasavada, The anatomy and biomechanics of acute and chronic whiplash injury, *Traffic Inj. Prev.* 10 (2009) 101–112, doi:[10.1080/15389580802593269](https://doi.org/10.1080/15389580802593269).
- [127] S.K. Ha, Finite element modeling of multi-level cervical spinal segments (C3–C6) and biomechanical analysis of an elastomer-type prosthetic disc, *Med. Eng. Phys.* 28 (2006) 534–541, doi:[10.1016/j.medengphy.2005.09.006](https://doi.org/10.1016/j.medengphy.2005.09.006).
- [128] N. Kallemeyn, A. Gandhi, S. Kode, K. Shivanna, J. Smucker, N. Grosland, Validation of a C2–C7 cervical spine finite element model using specimen-specific flexibility data, *Med. Eng. Phys.* 32 (2010) 482–489, doi:[10.1016/j.medengphy.2010.03.001](https://doi.org/10.1016/j.medengphy.2010.03.001).
- [129] J.B. Fice, D.S. Cronin, Investigation of whiplash injuries in the upper cervical spine using a detailed neck model, *J. Biomech.* 45 (2012) 1098–1102, doi:[10.1016/j.jbiomech.2012.01.016](https://doi.org/10.1016/j.jbiomech.2012.01.016).
- [130] A. Breig, A.F. el-Nadi, Biomechanics of the cervical spinal cord. Relief of contact pressure on and overstretching of the spinal cord, *Acta Radiol. Diagn. (Stockh.)* 4 (1966) 602–624, doi:[10.1177/028418516600400602](https://doi.org/10.1177/028418516600400602).
- [131] H.D. Yao, M.Y. Svensson, H. Nilsson, Transient pressure changes in the vertebral canal during whiplash motion—A hydrodynamic modeling approach, *J. Biomech.* 49 (2016) 416–422, doi:[10.1016/j.jbiomech.2016.01.005](https://doi.org/10.1016/j.jbiomech.2016.01.005).
- [132] H.D. Yao, M.Y. Svensson, H. Nilsson, Deformation of dorsal root ganglion due to pressure transients of venous blood and cerebrospinal fluid in the cervical vertebral canal, *J. Biomech.* 76 (2018) 16–26, doi:[10.1016/j.jbiomech.2018.05.012](https://doi.org/10.1016/j.jbiomech.2018.05.012).